Proton acceleration in thermonuclear nova explosions revealed by gamma rays

V. A. Acciari[1], S. Ansoldi[2,42], L. A. Antonelli[3], A. Arbet Engels[15], M. Artero[5], K. Asano[6], D. Baack[7], A. Babić[8], A. Baquero[9], U. Barres de Almeida[10], J. A. Barrio[9], I. Batković[11], J. Becerra González[1], W. Bednarek[12], L. Bellizzi[13], E. Bernardini[14], M. Bernardos[11], A. Berti[15], J. Besenrieder[15], W. Bhattacharyya[14], C. Bigongiari[3], A. Biland[4], O. Blanch[5], H. Bökenkamp[7], G. Bonnoli[16], Ž. Bošnjak[8], G. Busetto[11], R. Carosi[17], G. Ceribella[15], M. Cerruti[18], Y. Chai[15], A. Chilingarian[19], S. Cikota[8], S. M. Colak[5], E. Colombo[1], J. L. Contreras[9], J. Cortina[20], S. Covino[3], G. D'Amico[15,43], V. D'Elia[3], P. Da Vela[17,44], F. Dazzi[3], A. De Angelis[11], B. De Lotto[2], A. Del Popolo[21], M. Delfino[5,45], J. Delgado[5,45], C. Delgado Mendez[20], D. Depaoli[22], F. Di Pierro[22], L. Di Venere[23], E. Do Souto Espiñeira[5], D. Dominis Prester[24], A. Donini[2], D. Dorner[25], M. Doro[11], D. Elsaesser[7], V. Fallah Ramazani[26,46], L. Fariña Alonso[5], A. Fattorini[7], M. V. Fonseca[9], L. Font[27], C. Fruck[15], S. Fukami[4], Y. Fukazawa[28], R. J. García López[1], M. Garczarczyk[14], S. Gasparyan[29], M. Gaug[27], N. Giglietto[23], F. Giordano[23], P. Gliwny[12], N. Godinović[30], J. G. Green[15], D. Green[15*], D. Hadasch[6], A. Hahn[15], T. Hassan[20], L. Heckmann[15], J. Herrera[1], J. Hoang[9,47], D. Hrupec[31], M. Hütten[6], T. Inada[6], K. Ishio[12], Y. Iwamura[6], I. Jiménez Martínez[20], J. Jormanainen[26], L. Jouvin[5], D. Kerszberg[5], Y. Kobayashi[6], H. Kubo[32], J. Kushida[33], A. Lamastra[3], D. Lelas[30], F. Leone[3], E. Lindfors[26], L. Linhoff[7], S. Lombardi[3], F. Longo[2,48], R. López-Coto[11*], M. López-Moya[9], A. López-Oramas[1*], S. Loporchio[23], B. Machado de Oliveira

Fraga[10], C. Maggio[27], P. Majumdar[34], M. Makariev[35], M. Mallamaci[11], G. Maneva[35], M. Manganaro[24], K. Mannheim[25], L. Maraschi[3], M. Mariotti[11], M. Martínez[5], A. Mas Aguilar[9], D. Mazin[6,49], S. Menchiari[13], S. Mender[7], S. Mićanović[24], D. Miceli[2,50], T. Miener[9], J. M. Miranda[13], R. Mirzoyan[15], E. Molina[18], A. Moralejo[5], D. Morcuende[9], V. Moreno[27], E. Moretti[5], T. Nakamori[36], L. Nava[3], V. Neustroev[37], M. Nievas Rosillo[1], C. Nigro[5], K. Nilsson[26], K. Nishijima[33], K. Noda[6], S. Nozaki[32], Y. Ohtani[6], T. Oka[32], J. Otero-Santos[1], S. Paiano[3], M. Palatiello[2], D. Paneque[15], R. Paoletti[13], J. M. Paredes[18], L. Pavletić[24], P. Peñil[9], M. Persic[2,51], M. Pihet[15], P. G. Prada Moroni[17], E. Prandini[11], C. Priyadarshi[5], I. Puljak[30], W. Rhode[7], M. Ribó[18], J. Rico[5], C. Righi[3], A. Rugliancich[17], N. Sahakyan[29], T. Saito[6], S. Sakurai[6], K. Satalecka[14], F. G. Saturni[3], B. Schleicher[25], K. Schmidt[7], T. Schweizer[15], J. Sitarek[6]*, I. Šnidarić[38], D. Sobczynska[12], A. Spolon[11], A. Stamerra[3], J. Strišković[31], D. Strom[15], M. Strzys[6], Y. Suda[28], T. Surić[38], M. Takahashi[6], R. Takeishi[6], F. Tavecchio[3], P. Temnikov[35], T. Terzić[24], M. Teshima[15,52], L. Tosti[39], S. Truzzi[13], A. Tutone[3], S. Ubach[27], J. van Scherpenberg[15], G. Vanzo[1], M. Vazquez Acosta[1], S. Ventura[13], V. Verguilov[35], C. F. Vigorito[22], V. Vitale[40], I. Vovk[6], M. Will[15], C. Wunderlich[13], T. Yamamoto[41], D. Zarić[30], F. Ambrosino[53], M. Cecconi[54], G. Catanzaro[55], C. Ferrara[55], A. Frasca[55], M. Munari[55], L. Giustolisi[55], J. Alonso-Santiago[55], M. Giarrusso[56], U. Munari[57] and P. Valisa[58]

[1] Instituto de Astrofísica de Canarias and Dpto. de Astrofísica, Universidad de La Laguna, E-38200, La Laguna, Tenerife, Spain.
[2] Università di Udine and INFN Trieste, I-33100 Udine, Italy.
[3] National Institute for Astrophysics (INAF), I-00136 Rome, Italy.
[4] ETH Zürich, CH-8093 Zürich, Switzerland.
[5] Institut de Física d'Altes Energies (IFAE), The Barcelona Institute of Science and Technology (BIST), E-08193 Bellaterra (Barcelona), Spain.

[6] Japanese MAGIC Group: Institute for Cosmic Ray Research (ICRR), The University of Tokyo, Kashiwa, 277-8582 Chiba, Japan.
[7] Technische Universität Dortmund, D-44221 Dortmund, Germany.
[8] Croatian MAGIC Group: University of Zagreb, Faculty of Electrical Engineering and Computing (FER), 10000 Zagreb, Croatia.
[9] IPARCOS Institute and EMFTEL Department, Universidad Complutense de Madrid, E-28040 Madrid, Spain.
[10] Centro Brasileiro de Pesquisas Físicas (CBPF), 22290-180 URCA, Rio de Janeiro (RJ), Brazil.
[11] Università di Padova and INFN, I-35131 Padova, Italy.
[12] University of Lodz, Faculty of Physics and Applied Informatics, Department of Astrophysics, 90-236 Lodz, Poland.
[13] Università di Siena and INFN Pisa, I-53100 Siena, Italy.
[14] Deutsches Elektronen-Synchrotron (DESY), D-15738 Zeuthen, Germany.
[15] Max-Planck-Institut für Physik, D-80805 München, Germany.
[16] Instituto de Astrofísica de Andalucía-CSIC, Glorieta de la Astronomía s/n, 18008, Granada, Spain.
[17] Università di Pisa and INFN Pisa, I-56126 Pisa, Italy.
[18] Universitat de Barcelona, ICCUB, IEEC-UB, E-08028 Barcelona, Spain.
[19] Armenian MAGIC Group: A. Alikhanyan National Science Laboratory, 0036 Yerevan, Armenia.
[20] Centro de Investigaciones Energéticas, Medioambientales y Tecnológicas, E-28040 Madrid, Spain.
[21] INFN MAGIC Group: INFN Sezione di Catania and Dipartimento di Fisica e Astronomia, University of Catania, I-95123 Catania, Italy.
[22] INFN MAGIC Group: INFN Sezione di Torino and Università degli Studi di Torino, I-10125 Torino, Italy.
[23] INFN MAGIC Group: INFN Sezione di Bari and Dipartimento Interateneo di Fisica dell'Università e del Politecnico di Bari, I-70125 Bari, Italy.
[24] Croatian MAGIC Group: University of Rijeka, Department of Physics, 51000 Rijeka, Croatia.
[25] Universität Würzburg, D-97074 Würzburg, Germany.

[26] Finnish MAGIC Group: Finnish Centre for Astronomy with ESO, University of Turku, FI-20014 Turku, Finland.
[27] Departament de Física, and CERES-IEEC, Universitat Autònoma de Barcelona, E-08193 Bellaterra, Spain.
[28] Japanese MAGIC Group: Physics Program, Graduate School of Advanced Science and Engineering, Hiroshima University, 739-8526 Hiroshima, Japan.
[29] Armenian MAGIC Group: ICRANet-Armenia at NAS RA, 0019 Yerevan, Armenia.
[30] Croatian MAGIC Group: University of Split, Faculty of Electrical Engineering, Mechanical Engineering and Naval Architecture (FESB), 21000 Split, Croatia.
[31] Croatian MAGIC Group: Josip Juraj Strossmayer University of Osijek, Department of Physics, 31000 Osijek, Croatia.
[32] Japanese MAGIC Group: Department of Physics, Kyoto University, 606-8502 Kyoto, Japan.
[33] Japanese MAGIC Group: Department of Physics, Tokai University, Hiratsuka, 259-1292 Kanagawa, Japan.
[34] Saha Institute of Nuclear Physics, HBNI, 1/AF Bidhannagar, Salt Lake, Sector-1, Kolkata 700064, India.
[35] Inst. for Nucl. Research and Nucl. Energy, Bulgarian Academy of Sciences, BG-1784 Sofia, Bulgaria.
[36] Japanese MAGIC Group: Department of Physics, Yamagata University, Yamagata 990-8560, Japan.
[37] Finnish MAGIC Group: Astronomy Research Unit, University of Oulu, FI-90014 Oulu, Finland.
[38] Croatian MAGIC Group: Ruđer Bošković Institute, 10000 Zagreb, Croatia.
[39] INFN MAGIC Group: INFN Sezione di Perugia, I-06123 Perugia, Italy.
[40] INFN MAGIC Group: INFN Roma Tor Vergata, I-00133 Roma, Italy.
[41] Japanese MAGIC Group: Department of Physics, Konan University, Kobe, Hyogo 658-8501, Japan.
[42] also at International Center for Relativistic Astrophysics (ICRA), Rome, Italy.
[43] now at Department for Physics and Technology, University of Bergen, NO-5020, Norway.
[44] now at University of Innsbruck.

[45] also at Port d'Informació Científica (PIC), E-08193 Bellaterra (Barcelona), Spain.
[46] now at Ruhr-Universität Bochum, Fakultät für Physik und Astronomie, Astronomisches Institut (AIRUB), 44801 Bochum, Germany.
[47] now at Department of Astronomy, University of California Berkeley, Berkeley CA 94720.
[48] also at Dipartimento di Fisica, Università di Trieste, I-34127 Trieste, Italy.
[49] Max-Planck-Institut für Physik, D-80805 München, Germany.
[50] now at Laboratoire d'Annecy de Physique des Particules (LAPP), CNRS-IN2P3, 74941 Annecy Cedex, France.
[51] also at INAF Trieste and Dept. of Physics and Astronomy, University of Bologna, Bologna, Italy.
[52] Japanese MAGIC Group: Institute for Cosmic Ray Research (ICRR), The University of Tokyo, Kashiwa, 277-8582 Chiba, Japan.
[53]INAF - Osservatorio Astrofisico di Roma Via Frascati 33, IâĂŞ00078, Monteporzio Catone (Roma) Italy.
[54]INAF - Fund. Galileo Galilei Rambla José Ana Fernández Perez 7, 38712 Brenã Baja (La Palma), Canary Islands, Spain.
[55]INAF âĂŞ Osservatorio Astrofisico di Catania, Via S. Sofia 78, 95123 Catania, Italy.
[56]INFN - Laboratori Nazionali del Sud, Via S. Sofia 62, IâĂŞ95123 Catania, Italy.
[57]INAF - Osservatorio Astronomico di Padova, I-36012 Asiago (Vi), Italy.
[58]ANS Collaboration, c/o Astronomical Observatory, I-36012 Asiago (VI), Italy.

*Corresponding author(s). E-mail(s): contact.magic@mpp.mpg.de: J. Sitarek, R. López-Coto, D. Green, A. López-Oramas;

Classical novae are cataclysmic binary star systems in which the matter of a companion star is accreted on a white dwarf (WD) [1, 2]. Accumulation of hydrogen in a layer eventually causes a thermonuclear explosion on the surface of the WD [3], brightening the WD to $\sim 10^5$ solar luminosities and triggering ejection of the accumulated

matter. They provide extreme conditions required to accelerate particles, electrons or protons, to high energies. Here we present the detection of gamma rays by the MAGIC telescopes from the 2021 outburst of RS Ophiuchi (RS Oph), a recurrent nova with a red giant (RG) companion, that allowed us, for the first time, to accurately characterize the emission from a nova in the 60 GeV to 250 GeV energy range. The theoretical interpretation of the combined *Fermi*-LAT and MAGIC data suggests that protons are accelerated to hundreds of GeV in the nova shock. Such protons should create bubbles of enhanced Cosmic Ray density, on the order of 10 pc, from the recurrent novae.

A symbiotic nova can be formed when the companion star of the WD is a RG. [4]. The ejecta of symbiotic novae expand within the dense wind of the RG companion. Novae outbursts usually last from weeks to months. While they are expected to repeat hundreds of times [5], the interval between subsequent events can be even hundreds of thousand years [6]. However, a subclass of objects called Recurrent Novae (RNe) allows one to observe such repeated outbursts over a human lifespan [7]. In our Galaxy, ten such objects are known in which the repetition of bursts has been seen within a century [6]. According to [8] for the symbiotic nova to become recurrent, its WD must be massive ($\geq$1.1 $M_\odot$).

Novae have been deeply studied in the optical and X-ray ranges for decades [6, 9–13], but only recently they have been shown as emitters of high-energy gamma-ray radiation: first in the case of symbiotic novae [14] and soon after with classical novae [15]. Though this clearly indicates that charged particles are accelerated to high energies in novae, their nature and radiation mechanism are not yet clear. In order to understand the acceleration mechanism of high-energy particles, it is crucial to measure the maximum energies of the emitted radiation. Until recently, all spectra of gamma-ray novae have been measured only up to $6 - 10$ GeV range [15] with no hint of emission at higher energies [16, 17].

RS Oph is a recurrent symbiotic nova with average time between major outbursts of 14.7 years [6]. The latest outburst, in August 2021, was promptly reported in optical [18] and high-energy (HE, $100\,\mathrm{MeV} < E < 10\,\mathrm{GeV}$) gamma rays by *Fermi*-LAT [19]. The optical emission showed similar behaviour to the 2006 outburst (see Extended Data Figure EDF 1.Following these alerts, MAGIC began observations of RS Oph as part of its nova follow-up program [17], on August 09, 2021 at 22:27 UT, i.e., about 1 day after the first optical and GeV detections. In parallel, the H.E.S.S. collaboration announced very-high-energy (VHE, $\gtrsim 100\,\mathrm{GeV}$) gamma rays from RS Oph [20]. The MAGIC observations reveal VHE emission contemporaneous to the *Fermi*-LAT and optical maxima, and a decrease below the VHE detection limit two weeks later (see Fig. 1). Details of the analysis can be found in Methods section A.1. The first four days of MAGIC observations (August 09-12) yield a VHE signal with a significance of $13.2\,\sigma$ (see EDF 2), spanning from 60 GeV to 250 GeV, well fitted by a single power-law ($\chi^2/N_{dof} = 5.9/5$).

Daily spectra are reconstructed (see EDF 3, Method sections A.1 and Supplementary section H) allowing us to track the evolution of the outburst.

The contemporaneous gamma-ray spectrum measured by *Fermi*-LAT and MAGIC can be described as a single, smooth component spanning from 50 MeV to 250 GeV. Intriguingly, while the GeV emission subsides with a halving time scale of ~ 2.2 days (see also Methods section A.2), the flux measured by MAGIC over the first four days is consistent with being constant ($\chi^2/\mathrm{N_{dof}} = 2.9/3$), see also EDF 4This suggests a migration of the gamma-ray emission towards higher energies, in line with an increase of the maximum energies of the parent particles. RS Oph is the gamma-ray nova with the highest flux and energy output to date, as shown by the comparison with the other *Fermi*-LAT detected novae presented in Supplementary section I. Therefore, the non-detection of previous novae at VHE range [16, 17] might be explained by the lack of sensitivity to dimmer eruptions, without the need to invoke any fundamental difference in the spectral energy distribution of RS Oph.

The conditions in novae are favourable for the acceleration and subsequent emission of radiation by both electrons and protons [15]. The expanding ejecta of a nova interacting with the interstellar medium (filled also with the dense RG wind in the case of symbiotic novae) will result in the formation of a shock wave. Moreover, the fast wind, induced by the nuclear burning on the surface of the WD, will catch up with the ejecta, causing an additional internal shock [21]. Recently, a correlation between optical and gamma-ray emission has further suggested that a substantial part of the novae explosion's power goes into shocks [22]. In such shocks, energetic electrons and protons can be produced (see Fig. 2). Gamma-ray emission can arise from photosphere thermal radiation up-scattered to the gamma-ray energy range by relativistic electrons via inverse Compton scattering. Alternatively, the ambient matter (nova ejecta and RG wind) can act as a target for hadronic interaction of protons or Bremsstrahlung radiation of electrons [15]. The maximum energies of high-energy particles will depend on the efficiency of the acceleration mechanism, duration of the nova, and the cooling energy losses (see Methods section B.1 and EDF 5). Protons experience only mild cooling by proton-proton interactions with time scale of $t_{pp} = 21(n_p/6\times10^8\,\mathrm{cm}^{-3})^{-1}$ [day], where n_p is the number density of the target material. Electrons in nova shocks suffer stronger inverse Compton energy losses with $t_{IC} = 4.4\times10^{-3}(E/300\,\mathrm{GeV})^{-1})[1+10(E/300\,\mathrm{GeV})]^{1.5}$ [day]. Therefore, the production of high energy photons via leptonic mechanisms is much more demanding on the acceleration processes efficiency than for proton models. The simultaneous acceleration of both types of particles (but reaching different energies) has also been proposed [17, 23]. We estimate that Bremsstrahlung is negligible with respect to inverse Compton component for the parameters of RS Oph (see Methods section B).

We derive the photosphere parameters using fits to the photometry measurements (see EDF 6) and shock expansion velocity from spectroscopy (see

EDF 7). Based on the optical observations of RS Oph during the 2021 outburst, and the derived parameters from previous outbursts of the source, we model the gamma-ray emission with the injection of a population of relativistic electrons or protons (see Methods section B). We take into accout also the minor absorption of the emission in the photosphere radiation field (see EDF 8). The *Fermi*-LAT and MAGIC measurement can be well described ($\chi^2/\mathrm{N_{dof}} = 13.1/12$, p-value = 0.36) with the proton-only model (see left panel of Fig. 3).

The fit yields a canonical power-law spectrum with an index ~ -2 and an exponential cut-off, corresponding to the maximum energies achieved in the acceleration. The day-by-day modeling shows evidence that the energy cut-off of protons increases with time (see Supplementary section H and EDF 9). This goes in line with absence of spectral signatures from cooling terms. The associated neutrino emission is not expected to be detected by the current experiments (see Supplementary section F).

In contrast, it is difficult to explain the shape of the curvature of the measured spectrum between 50 MeV and 250 GeV with leptonic processes. The leptonic model requires injection of particles that already contain a strong break (change of particles index by 3.25 ± 0.28) in the electron energy distribution (see Fig. 3, right panel). Since the break must already be present in the injection spectrum of particles, it cannot be explained by the cooling. In addition, despite a more complicated particle injection model, the description of the gamma-ray emission in the electron scenario is significantly worse ($\chi^2/\mathrm{N_{dof}} = 27.5/11$, p-value $= 3.9 \times 10^{-3}$) than in the case of protons, as can be seen in Fig. 3. The relative likelihood of the electron model with respect to the proton model for ΔAIC= 15.3, as defined within the Akaike information criterion framework [24], which is normally used for comparison of non-nested models, is 4.7×10^{-4}.

Despite their intense emission of gamma rays, accelerated protons will eventually escape the nova shock carrying away most of their obtained energy. Such protons can contribute to the Galactic Cosmic Rays (CR), which are expected to be produced mainly in supernova remnants [25].

The measurement of the proton spectrum required to explain the gamma-ray emission of RS Oph can be used to put estimates on novae contribution to CR. Using the CR energetics derived for RS Oph ($\sim 4.4 \times 10^{43}$ erg, see Methods section B.2), a rate of 50 novae per year [26] would lead to about 0.1% of the CR energy contribution from supernovae, which are more rare than novae ($\sim$ 2 per century) but much more energetic ($\sim 10^{50}$ erg). Despite the small contribution to the overall CR sea, a nova would significantly increase the CR density in its close environment. The energy density of the nova dominates over that of the average CR energy density in the Milky Way ($\sim$1.8 eV/cm^3) in a region of radius $\sim$0.5 pc, of the order of the distance to the nearest star in our Galaxy. In the special case of recurrent novae, protons accelerated over 10^5 yr [27], assuming a recurrent rate of every 15 years, will accumulate in a $\sim$ 9 pc bubble with enhanced CR density (see Methods section B.2.1).

The detection of gamma rays reaching 250 GeV from a recurrent symbiotic nova allowed us to obtain a deep physical insight on the population of relativistic particles accelerated by such objects. The modeling of the gamma-ray spectrum strongly favors the explanation of the emission via the acceleration of protons in a nova shock. Evidence towards the proton acceleration is based on: (i) the inferred shape of the energy distribution of injected particles, (ii) the better statistical description of the gamma-ray spectral energy distribution by the proton model, (iii) the obtained evidence of the increase of the particle maximum energies over time, consistent with lack of strong cooling. The protons in the nova shock undergo slow cooling, therefore they will be eventually able to escape the shock, carrying away a significant fraction of energy. Such protons will add to the Galactic cosmic ray budget, however primarily in the close neighborhood of novae.

The observation of the August 2021 outburst of RS Oph introduces a new class of sources as VHE gamma-ray emitter: (recurrent symbiotic) novae. RS Oph is a recurrent symbiotic nova, the same class of objects as V407 Cyg, the first nova detected in the GeV range by *Fermi*-LAT. While we now know that classical novae are also GeV emitters, it is still to be seen if the detection of RS Oph emitting in VHE gamma-ray range is due to its recurrent symbiotic nature, or just the first sign of such emission from a broader class of classical novae. The comparison of gamma-ray measurements in GeV and VHE gamma-ray range with previous *Fermi*-LAT novae does not reveal any peculiarity in the emission of RS Oph, except for its brightness (see Fig. 4 and EDF 10). Therefore, it is likely that future, more sensitive VHE gamma-ray facilities will be able to provide an ample harvest of novae.

Methods

A Observations and data analysis

In this section we report the detailed results of the analysis of gamma-ray data with MAGIC and *Fermi*-LAT, and optical data with TJO and ANS.

A.1 MAGIC

MAGIC [28] is a stereoscopic system of two imaging atmospheric Cherenkov telescopes situated in the Canary island of La Palma, Spain (28.8°N, 17.9°W at 2225 m above sea level). Each telescope consists of a 17-m diameter mirror dish and a fast imaging camera. The system achieves a sensitivity of $(0.92 \pm 0.04)\%$ of the Crab Nebula flux above 210 GeV in 50 h in zenith angle range $30 - 45°$ [29].

MAGIC observed RS Oph in the period between August 09, 2021 to September 01, 2021 (MJD 59435.94 to 59458.97) for 34.0 h (see Supplementary Table 2). The data quality selection was based on the atmospheric transmission and rates of background events. For this analysis we also did not include data taken under moonlight condition, as they provide much higher energy threshold values. After quality cuts, 21.4 h of the data were used for the analysis, half of which were taken during the first four days after the nova eruption. The source was observed at zenith angles between 36° and 60°. The data were taken in the so-called wobble mode, pointing at four different sky positions situated 0.4° away from the source to evaluate the background simultaneously.

The data were analyzed using the MAGIC Analysis and Reconstruction Software, MARS [30]. A dedicated low-energy procedure with a special signal extraction and image cleaning, the so-called MaTaJu method, was applied (see [31] and references therein). Further processing of the data, including the image parameterization, the direction and energy reconstruction and gamma-hadron separation, were applied following the standard MARS analysis chain. The energy threshold of the analysis is ∼60 GeV.

We fitted the spectrum obtained from the first four days of observations using a single power-law ($\mathrm{d}N/\mathrm{d}E = f_0\ (E/E_0)^{-\alpha}$), resulting with a $\chi^2/\mathrm{N_{dof}} = 5.9/5$ goodness of fit. The used fit also takes into account estimated energy bins without detected signal, hence the number of degrees of freedom is larger than expected from the number of points in the reconstructed spectrum. The normalization energy of the fit ($E_0 = 130\,\mathrm{GeV}$) is the decorrelation energy (i.e. normalization energy which minimizes the correlation of the fit parameters) of the four-day sample. The fit parameters are listed in Supplementary Table 3.

In order to estimate the lower limit on the maximal true energy of gamma rays consistent with the MAGIC data we follow the procedure of [32]. We perform a likelihood fit of the data with a power-law model with a sharp cut-off at a given energy E_{cut}. The 3σ (99.7% C.L.) lower limit on the E_{cut} is the value for which the increase of the χ^2 of the fit is equal to 9. We obtain 170 GeV, however taking into account also the 15% systematic uncertainty on the energy scale following [29] we obtain a slightly less constraining, conservative limit of $E_{cut} > 150\,\mathrm{GeV}$.

We have also performed night-by-night spectral fits to investigate spectral variability. The parameters from the first two nights are consistent within errors (note however that the exposure on the first night is lower than on the remaining ones). A hint of hardening of the emission is seen between the second and third night. No significant change of parameters can be seen between the third and the fourth night.

The daily-binned light curve was calculated for an integral flux above 100 GeV. For the first four days the fit to a constant flux gives a $\chi^2/\mathrm{N_{dof}} = 2.9/3$ with a value of $F_0 = (4.41 \pm 0.46_{\mathrm{stat}}) \times 10^{-11}\,\mathrm{cm^{-2}\,s^{-1}}$.

A.2 *Fermi*-LAT

The Large Area Telescope on-board the *Fermi* Gamma-ray Space Telescope (*Fermi*-LAT), is a pair conversion telescope designed to detect gamma rays with an energy range of 0.02 GeV to > 300 GeV [33]. The *Fermi*-LAT, with its large field of view (2.4 sr), observes the entire sky approximately every 3 hours. Each analysis is performed with *fermitools* v2.0.8 and *Fermipy* v1.0.2 [34] using a binned likelihood analysis, P8R3_V3 instrument response functions (IRFs), and the catalog 4FGL-DR2 [35, 36] with the standard Galactic and isotropic diffuse background to construct the model of the region of interest (ROI). For each analysis, the *SOURCE* event class is used as this is the recommended event class for long duration observations, observations of more than a few hours. The *SOURCE* event class can be further divided into separate event types such as *PSF0*, *PSF1*, *PSF2*, and *PSF3*, where *PSF0* corresponds to events with the worst PSF and *PSF3* are events with the best PSF.

For the 1-day and 3-day time bins, the *Fermi*-LAT data-set used encompasses a total time range from MJD 59431.45 to 59461.45, an energy range from 0.1 GeV to 1000 GeV, and a 15° ROI centered on the radio coordinates of RS Oph (R.A. = 267.555°, Dec. = -6.7078°). We use event type 3, which corresponds to all events, for this analysis and select a maximum zenith angle of > 90° to reduce any gamma-ray contamination from the Earth limb. The majority of 4FGL-DR2 sources for the one and three day time bins are not significantly detected (Test Statistic (TS) > 25, see [37]), apart from 4FGL J1813.4-1246 and 4FGL J1745.4-0753. These sources correspond to PSR J1813-1246 and TXS 1742-078, which are 8.3° and 1.7° away from RS Oph. Here, TS is defined as TS = -2 ln $(\mathcal{L}_{max,0}/\mathcal{L}_{max,1})$, where $\mathcal{L}_{max,0}$ is the maximum likelihood of the null hypothesis and $\mathcal{L}_{max,1}$ is the maximum likelihood with the source included [37]. The square-root of the TS is approximately equal the significance of detection, i.e. a TS = 25 is $\sim 5\,\sigma$. TXS 1742-078 is a non-variable hard blazar and therefore could cause possible source confusion. Due to the proximity of 4FGL J1745.4-0753 to RS Oph and possible source confusion at the lowest energies, the value of the index of 4FGL J1745.4-0753 is locked to that of the 4FGL-DR2 catalog. RS Oph is included in the ROI and modeled with a Log Parabola model. Additional spectral models were tested for a four-day period contemporaneous to MAGIC observations: a power-law (TS= 2168.1) as well as a power-law with an exponential cutoff (TS= 2016.4), and the Log Parabola model (TS= 2226.44) had the highest TS, and therefore we use the Log Parabola model as our spectral form for RS Oph. The ROI is optimized with the normalization and spectral parameters of any 4FGL-DR2 source with a number of predicted counts < 1 locked to the 4FGL-DR2 values, excluding the Galactic and isotropic diffuse background. All parameters on all unlocked 4FGL-DR2 sources within 4° are left free to vary, and the ROI is fit using *Minuit* minimizer. If RS Oph source model does not have a TS > 9, number of predicted counts > 4 or the error of the integrated flux from 0.1 GeV to 1000 GeV is greater than 60% of the value, then it is not considered detected and 95% upper limits (ULs) are calculated. These 1-day and 3-day light curves are presented in Supplementary Tables 4 and 5 and in Fig. 1. The 1-day light curve in MJD 59435.45–59444.45 range can be well fit ($\chi^2/\mathrm{N_{dof}} = 6.5/7$) with an exponential decay with halving time of (2.20 ± 0.18) days.

The analysis of the combined first four days has a data-set which encompasses a time range MJD 59435.45 – 59439.45 and an energy range from 0.05 GeV to 1000 GeV. Reaching down to 0.05 GeV is necessary to help distinguish leptonic and hadronic models described in the main text and seen in Fig. 3. The same procedure is applied as in the 1-day and 3-day time bins, with some adjustments in the settings to allow the analysis to reach 0.05 GeV. Due to the worsening of the *Fermi*-LAT PSF below 0.1 GeV, we apply a 20° ROI centered on RS Oph, and a more restrictive zenith angle selection of $> 80°$. We perform a joint-likelihood analysis with two components, one in the energy range between 0.05 GeV to 0.1 GeV and one in the energy range from 0.1 GeV to 1000 GeV. We remove *PSF0* and *PSF1* event types from the analysis below 0.1 GeV and keep all event types above 0.1 GeV. *PSF0* and *PSF1* are events classified with poor PSF and removing these event types thereby improves the PSF with the trade-off of less data. This reduces the possibility of source confusion from nearby weak sources. This also reduces the chance of false positive detections as described in the *Fermi*-LAT low energy catalog (1FLE)[38].

A.3 Optical photometry

Optical photometric observations of RS Oph were carried out by Joan Oró Telescope (TJO) and *Asiago Novae & Symbiotic stars Collaboration* (ANS, telescopes ID 310, 610 and 2203). The TJO is a 1-meter class robotic telescope located at Montsec observatory (42.05°N, 0.73°E), Catalonia, Spain. The multi band (BVR_cI_c) data were analysed using a semi-automatic pipeline for differential photometry [39] assuming the aperture radius of 7.5″. The comparison stars magnitudes are obtained from American Association of Variable Star Observers International Database (AAVSO). The stars are numbered as 115, 121, 129, 130, and 133 in the database finding chart.

The data obtained by ANS are analyzed using PSF photometry method described in [40, 41]. The same local photometric sequence, extracted from APASS DR8 all-sky survey [42, 43] and accurately placed on the system of equatorial standards [44] via the color equations calibrated in [45, 46], has been used for all telescopes ensuing a high consistency of the data. The photometry results are given in Supplementary Table 6, where the quoted uncertainties are the total error, which quadratically combine the measurement error on the variable with the error associated to the transformation from the instantaneous local photometric system to the standard one (as defined by the photometric comparison sequence). All measurements were carried out with aperture photometry.

The cross calibration between instruments was performed by using the color index of the source. The data obtained by two telescopes are in good agreement. However, to reduce the systematic uncertainties, minimal offsets ($B - V = +0.03$, $V - R_c = +0.05$, and $V - I_c = -0.02$) were applied to TJO data. The contribution of the strongest emission lines (H_α and H_β) were removed from the observed magnitude using the simultaneous spectroscopic observations from the publicly available optical spectra in Astronomical Ring for Access to Spectroscopy (ARAS) [47]. We found that the contribution of the H_β emission line in the V-band is negligible for the first ten days after the outburst. The contribution of the H_β emission line is significant in the B-band and increases from 3% to 15% during the same time interval. Moreover, the contribution of the H_α emission line is dominant in the R-band and increases from 5% to 83% during the same time interval owing to a sudden jump from 5% to 34% between $T - T_0 = 0.98$ days and $T - T_0 = 2.89$ days. The results of these corrections are presented in Supplementary Table 7.

All optical data described in this section are corrected for the effect of Galactic extinction by assuming $E(B-V) = 0.65$ [48], Galactic extinction law [49], and the absolute fluxes (corresponding to zero magnitude) [50] in each band.

During the nova outburst the photosphere emission creates the dominant radiation field. We describe the radiation field using photometric and spectroscopic measurements by applying black body approximation. During the first four days of the nova, contemporaneous with the MAGIC measurements, the emission can be described by the photosphere temperature dropping from $T_{ph} = 10800\,\mathrm{K}$ to $7680\,\mathrm{K}$ and radius $R_{ph} = 200\,R_\odot$ (see EDF 6). It should be noted that the asymmetry of the photosphere (see e.g. [51, 52], lack of measurements at the shortest wavelengths and the presence of lines affect the above mentioned fits. Therefore, the photosphere radius and temperature values should be considered only a crude approximation of the radiation field, in context of gamma-ray emission, and no conclusion on the evolution of those two parameters should be drawn. Noteworthly, the photosphere fit of 2006 eruption [52], when rescaled to the nova distance of 2.45 kpc, provides a similar radius $(245 - 310)\,R_\odot$, and temperature (8200 K).

A.4 Spectroscopy and ejecta kinematics

RS Oph spectra during the 2021 outburst have been acquired with the Echelle spectrograph of the Varese 0.84 m telescope [53] and the Catania Astrophysical Observatory Spectropolarimeter [54] of the Catania 0.91 m telescope. The reduction of spectra, which included the subtraction of the bias frame, trimming, correcting for the flat-field and the scattered light, extraction for the orders, and wavelength calibration, was done as in [55] by using the NOAO/IRAF packages. IRAF is distributed by the National Optical Astronomy Observatory, which is operated by the Association of Universities for Research in Astronomy, Inc.

The H_α profile obtained on day $T - T_0 = 0.91$ consists of a triangular shape with Full Width at Zero Intensity of $\sim 7500\,\mathrm{km\,s^{-1}}$ and a blue shift absorption component at $4250\,\mathrm{km\,s^{-1}}$, exactly as it was reported by [56] 1.38 days after the 2006 outburst of RS Oph.

The close similarity of the 2006 and 2021 spectral line profiles along the envelope expansion is testified on day $T - T + 0 = 15$ by the presence of satellite components at the same high-velocity ($2500\,\mathrm{km\,s^{-1}}$). This feature was associated by [56] to a presence of two jets (c.f. figs. 1 and 2 therein and EDF 7). Also, [57] measured a velocity of $4200\,\mathrm{km\,s^{-1}}$ the day after the outburst.

Because of the day-by-day changing of absorption and emission features across the whole RS Oph spectrum, we have determined the velocity of the expanding envelope as the terminal value simultaneously representative of the H_α, H_β and He I 5876λ P-Cygni profiles (Supplementary Table 8). An error of 250 $\mathrm{km\,s^{-1}}$ was assumed as representative of differences between profiles. EDF 7 shows these profiles in the first three days after the expansion as well as on days 5 and 15.

The acceleration along the initial three days is not statistically confirmed and we assume $(4500 \pm 250)\,\mathrm{km\,s^{-1}}$ as representative of the ejecta expansion at the earliest stage (during the VHE gamma-ray detection by MAGIC).

It is worth to remind that this velocity is volume average, weighted by the brightness, temperature and density of the ejecta velocities and agrees with results from the modeling by [58] of the HST images of the spatially resolved and expanding ejecta during the 2006 event. Radio maps of the 2006 outburst of RS Oph [59] have shown the presence of highly collimated flows with a velocity close to 10000 $\mathrm{km\,s^{-1}}$. In this framework, the decrement of the velocity after the initial days is simply a consequence of a non-spherical mass outflow [56, 58, 60].

B Modeling

There are compelling both simulation (see e.g. [61]) and observational (see e.g. [60]) evidence that the mass transfer in symbiotic binaries causes non-spherical circumstellar environment. Such asymmetries are crucial when considering the morphology of the emission in particular in optical and X-ray ranges. Here, using a similar approach to [17, 23], we consider a simplified, spherically-symmetric scenario in order to evaluate the conditions in which gamma-ray radiation can be produced by either electrons or protons and to investigate spectral features of such an emission. The used parameters are summarized in Supplementary Table 10

B.1 Acceleration and cooling of particles

We parametrize the acceleration of charged particles with acceleration parameter ξ:

$$\left(\frac{dE}{dt}\right)_{acc} = \frac{\xi c E}{R_L(E)}, \tag{1}$$

where $R_L(E)$ is the Larmor radius of particle with energy E in perpendicular magnetic field B. The corresponding acceleration time scale, expressed in days, can be computed as:

$$t_{acc} = E/\left(\frac{dE}{dt}\right)_{acc} = 3.9\left(\frac{E}{300\,\mathrm{GeV}}\right)\left(\frac{\xi B}{10^{-7}\,\mathrm{G}}\right)^{-1}\ [\mathrm{day}]. \tag{2}$$

The maximum achieved energies will stem from balancing such acceleration time with ballistic time t_{bal}, defined as the time from the onset of the nova, or by dominating cooling process. The shock distance R_{sh} at the time $t = T - T_0$ can be estimated based on its speed v_{sh}:

$$R_{sh} = 1.2\times 10^{14}\left(\frac{v_{sh}}{4500\,\mathrm{km\,s^{-1}}}\right)\left(\frac{t}{3\,\mathrm{d}}\right)\ [\mathrm{cm}]. \tag{3}$$

As the nova shock expands the adiabatic energy losses will be directly connected with the ballistic time. We define the adiabatic time scale as the time in which the energy of particles decreases by a factor of e, resulting in $t_{adiab} = e\, t_{bal}$.

The protons will cool on hadronic interactions with the ambient matter, either the nova ejecta, or the RG wind. We assume that the ejecta concentrate at the distance of R_{sh} in a layer with a thickness of $h \times R_{sh}$, with $h = 0.1$. The number density of the ejecta can be estimated as:

$$n_{ej} = \frac{M_{ej}}{4\pi h R_{sh}^3 m_p} = 6.0\times 10^8 \frac{M_{ej}}{10^{-6} M_\odot}\left(\frac{v_{sh}}{4500\,\mathrm{km\,s^{-1}}}\right)^{-3}\left(\frac{t}{3\,\mathrm{d}}\right)^{-3}\left(\frac{h}{0.1}\right)^{-1}\ [\mathrm{cm}^{-3}], \tag{4}$$

where M_{ej} is the total ejected mass and m_p is the proton mass. Alternative assumption that the ejecta fill homogenously a sphere with radius R_{sh} would result in a factor of 3 lower value of n_{ej}. The number density of the ambient material in the RG wind can be estimated as:

$$n_{RG} = \frac{\dot{M}_{RG}}{4\pi R_{sh}^2 v_{RG} m_p} \tag{5}$$

$$= 1.1\times10^{8}\frac{\dot{M}_{RG}}{5\times10^{-7}M_{\odot}/\mathrm{yr}}\Big(\frac{v_{sh}}{4500\,\mathrm{km\,s^{-1}}}\Big)^{-2}\Big(\frac{t}{3\,\mathrm{d}}\Big)^{-2}\Big(\frac{v_{RG}}{10\,\mathrm{km\,s^{-1}}}\Big)^{-1}[\mathrm{cm^{-3}}],$$

where v_{RG} is the speed of the RG wind and $\dot{M}_{RG}$ is the mass loss rate of the RG. The total density of the ambient medium for the hadronic interaction for the assumed parameters of RS Oph it is mostly dominated by the ejecta ($n_p \approx n_{ej}$). The proton cooling time scale on hadronic p-p interactions can be then computed as:

$$t_{pp} = (n_p c\sigma_{pp})^{-1} = 21(n_p/6\times10^{8}\,\mathrm{cm^{-3}})^{-1}\,[\mathrm{day}], \tag{6}$$

where $\sigma_{pp} = 3\times10^{-26}\,\mathrm{cm}^2$. As the cooling timescale is longer than the ballistic time, the maximum energies to which protons can be accelerated are determined by the time from the nova onset.

In the case of electrons, cooling losses can originate either from inverse Compton scattering on the photosphere thermal radiation or from Bremsstrahlung radiation on the ambient matter. We compute the inverse Compton cooling time scale taking into account Klein-Nishina correction factor following [62]

$$t_{IC} = \frac{3(m_e c^2)^2}{4c\sigma_T u_{ph} E}\left(1 + 4\epsilon_{ph}E/(m_e c^2)^2\right)^{1.5}, \tag{7}$$

where m_e is the electron mass. The total energy density, u_{ph}, and characteristic temperature of soft photons, ϵ_{ph}, can be estimated as

$$u_{ph} = 0.14\frac{(R_{ph}/200\,R_{\odot})^2(T_{ph}/8460\,\mathrm{K})^4}{(v_{sh}/4500\,\mathrm{km\,s^{-1}})^2(t/3\,\mathrm{d})^2}[\mathrm{erg\,cm^{-3}}] \tag{8}$$

$$\epsilon_{ph} = 2.2(T_{ph}/8460\,\mathrm{K})\,[\mathrm{eV}]. \tag{9}$$

For the used above scaling values the dependence of t_{IC} with energy can be described as $t_{IC} = 4.4\times10^{-3}(E/300\,\mathrm{GeV})^{-1})[1 + 10(E/300\,\mathrm{GeV})]^{1.5}\,[\mathrm{day}]$ resulting in fast cooling of high-energy electrons. We estimate the Bremsstrahlung losses using the same density of ambient matter n_p as

$$t_{brems} = X_0/(n_p m_p c) = 24(n_p/6\times10^{8}\,\mathrm{cm^{-3}})^{-1}\,[\mathrm{day}], \tag{10}$$

where $X_0 = 63\,\mathrm{g\,cm^{-2}}$ is the radiation length in proton gas. For the expected parameters of RS Oph, the Bremsstrahlung losses are thus negligible. Also the synchrotron energy losses are negligible, unless the magnetic field in the shock reaches the level of about 1 G.

In order to accelerate protons up to energies of a few hundred GeV, the value of $\xi B \gtrsim 10^{-7}\,\mathrm{G}$ is required (EDF 5). If electrons are accelerated in the same conditions, they can reach energies of only $\sim 10\,\mathrm{GeV}$. In order to explain the observed gamma-ray emission reaching hundreds of GeV, much higher values $\xi B \gtrsim 3 \times 10^{-6}$ G are required. Second-order Fermi acceleration on the nova shock is expected to provide acceleration parameter of the order of $\xi \lesssim (v_{sh}/c)^2 \approx 10^{-4}$, resulting in the requirement of $B \gtrsim 0.03\,\mathrm{G}$ fields for the electron case and much weaker $B \gtrsim \mathrm{mG}$ for the proton one.

B.2 Energetics

The kinetic energy of the ejecta can be estimated as:

$$E_k = 0.5 M_{ej} v_{sh}^2 = 2.0 \times 10^{44} \left(\frac{M_{ej}}{10^{-6} M_\odot}\right) \left(\frac{v_{sh}}{4500\,\mathrm{km\,s^{-1}}}\right)^2 \mathrm{erg} \tag{11}$$

For the assumed parameters determining the density of target material, the fit of the proton energy distribution in Fig. 3 requires a total power in protons of 4.4×10^{43} erg. This energetics requirement scales with the assumed model parameters as:

$$E_{p,nova} = 0.44 \times 10^{44} \left(\frac{M_{ej}}{10^{-6} M_\odot}\right)^{-1} \left(\frac{v_{sh}}{4500\,\mathrm{km\,s^{-1}}}\right)^3 \left(\frac{d}{2.45\mathrm{kpc}}\right)^{-2} \frac{h}{0.1}\,\mathrm{erg} \tag{12}$$

Therefore the efficiency of conversion of energy from the shock to protons can be computed as:

$$\epsilon = \frac{E_{p,nova}}{E_k} = 0.22 \left(\frac{M_{ej}}{10^{-6} M_\odot}\right)^{-2} \left(\frac{v_{sh}}{4500\,\mathrm{km\,s^{-1}}}\right) \left(\frac{d}{2.45\mathrm{kpc}}\right)^{-2} \frac{h}{0.1} \tag{13}$$

It is clear that protons need to obtain a significant fraction ($\sim 20\%$) of the shock kinetic energy. Lower fraction could be achieved if the mass of the ejecta is higher, it is more concentrated at the shock (lower h) or if the speed of the shock is decreased. Concentration of the nova ejecta and proton acceleration in the bipolar direction would increase the target material density and efficiency of the gamma ray production. This would further lower the total energy required in the accelerated protons compared to the assumed here spherically symmetric scenario.

B.2.1 Contribution to the Cosmic Ray sea

These accelerated protons eventually escape the nova to be part of the sea of Cosmic Rays. Since they do not suffer strong energy losses due to their interaction with intergalactic magnetic and photon fields, as it is the case for electrons, their contribution may extend to large distance from the nova explosion at all energies. Assuming that the energy released in all novae into accelerated protons is similar to that released in RS Oph ($E_{p,nova} = 4.4 \times 10^{43}$ erg) and a nova rate of $\sim$ 50 per year [26] we get a total of

$$\text{Novae energy rate} = E_{p,nova} \times \text{nova rate} = 2.2 \times 10^{45} [\text{erg/year}] \tag{14}$$

It is considered that a supernova explosion usually releases $E_{\rm SN} \sim 10^{51}$ erg [63], out of which ∼10% can be converted into accelerated protons at the shock between the supernova ejecta and the interstellar medium (ISM). The SN rate in the galaxy is ∼2 per century [64], therefore the supernova energy rate would be:

$$\text{Supernovae energy rate} = 0.1 \times E_{\rm SN} \times \text{supernova rate} = 2 \times 10^{48} [\text{erg/year}] \tag{15}$$

making the contribution of novae $\lesssim$0.2% to that of supernovae.

Let us now assume that the average energy density in CRs in the Milky Way is $E_{\rm dens,CRs}$ ∼1.8 eV/cm^3 [65]. We would like to compute what is the region in which the energy density of the protons accelerated by the nova dominates over this energy density. The energy density of these protons will be given by the total energy ($E_{p,nova}$) divided by the volume of the region

$$E_{\rm dens,nova,1\,eruption} = \frac{3E_{p,nova}}{4\pi R^3_{\rm eruption}} \tag{16}$$

where $R_{\rm eruption}$ is the radius of the region. If we compare $E_{\rm dens,nova} = E_{\rm dens,CRs}$, we obtain $R_{\rm eruption}$ ∼0.5 pc, that is subject to the assumption on the energy density performed and may change if larger energy densities are considered [66].

Finally, in the special case of a recurrent nova like RS Oph that repeats its explosions every ∼15 years [67], we would get this energy injection repeated over time. Considering a period of recurrence of up to 10^5 years, the region over which this nova would dominate has a size of:

$$E_{\rm dens,nova,recurrent} = \frac{3E_{p,nova} \times 10^4}{4\pi R^3_{\rm recurrent}} \tag{17}$$

and the radius over which the protons accelerated by the nova would dominate over the energy density of the ISM would be $R_{\rm recurrent}$ ∼9 pc.

Availability of data and materials: Analysis products of MAGIC data are available here: http://vobs.magic.pic.es/fits/. Low level data are available on request.

Code availability: The code for fitting the electron and proton models is available in https://opendata.magic.pic.es/download?pid=2.

Acknowledgments. We would like to thank the Instituto de Astrofísica de Canarias for the excellent working conditions at the Observatorio del Roque de los Muchachos in La Palma. The financial support of the German BMBF, MPG and HGF; the Italian INFN and INAF; the Swiss

National Fund SNF; the ERDF under the Spanish Ministerio de Ciencia e Innovación (MICINN) (PID2019-104114RB-C31, PID2019-104114RB-C32, PID2019-104114RB-C33, PID2019-105510GB-C31,PID2019-107847RB-C41, PID2019-107847RB-C42, PID2019-107847RB-C44, PID2019-107988GB-C22); the Indian Department of Atomic Energy; the Japanese ICRR, the University of Tokyo, JSPS, and MEXT; the Bulgarian Ministry of Education and Science, National RI Roadmap Project DO1-400/18.12.2020 and the Academy of Finland grant nr. 320045 is gratefully acknowledged. This work was also supported by the Spanish Centro de Excelencia "Severo Ochoa" (SEV-2016-0588, SEV-2017-0709, CEX2019-000920-S), the Unidad de Excelencia "María de Maeztu" (CEX2019-000918-M, MDM-2015-0509-18-2) and by the CERCA program of the Generalitat de Catalunya; by the Croatian Science Foundation (HrZZ) Project IP-2016-06-9782 and the University of Rijeka Project uniri-prirod-18-48; by the DFG Collaborative Research Centers SFB823/C4 and SFB876/C3; the Polish National Research Centre grant UMO-2016/22/M/ST9/00382; and by the Brazilian MCTIC, CNPq and FAPERJ. The Joan OrÃş Telescope (TJO) of the Montsec Observatory (OdM) is owned by the Catalan Government and operated by the Institute for Space Studies of Catalonia (IEEC). We acknowledge with thanks the variable star observations from the AAVSO International Database contributed by observers worldwide and used in this research. We gratefully acknowledge the prompt response to the alert and the data provided by the CAOS Team. We acknowledge with thanks the Astronomical Ring for Amateur Spectroscopy (ARAS) database [47] (https://aras-database.github.io/database/index.html). The observers who contributed worldwide and used in this research are Olivier Garde, Vincent Lecoq, Lorenzo Franco, Francois Teyssier, Olivier Thizy, Christophe Boussin, Pavol A. Dubovsky, and David Boyd. The authors would like to thank Giacomo Principe for the advice in extending the *Fermi*-LAT analysis below 100 MeV and Filippo D'Ammando for his comments on the manuscript. R.L-C.'s work was financially supported by the European Union's Horizon 2020 research and innovation program under the Marie SkÅĆodowska-Curie grant agreement No. 754496 - FELLINI. We would like to thank the anonymous journal reviewers for the comments that helped to improve the manuscript.

Author Contribution Statement: The individual authors who contributed to this manuscript in alphabetic order are W. Bednarek: theoretical interpretation; V. Fallah Ramazani: analysis and coordination of the optical photometry data, drafting of the corresponding paper section; D. Green: trigger of the MAGIC observations, analysis of the MAGIC data, drafting and edition of the manuscript; F. Leone: coordination and analysis of the optical spectroscopy data, interpretation of ejecta kinematics; R. López-Coto: analysis of the MAGIC and Fermi-LAT data, theoretical interpretation, comparison with other novae, computation of the contribution to CRs, drafting and edition of the manuscript; A. López-Oramas: trigger and coordination of the MAGIC campaign, analysis of the MAGIC data, drafting and edition of the manuscript;

U. Munari: analysis of the optical photometry data and cross-calibration of the different optical instruments; J. Sitarek: coordination of the MAGIC novae observation program, analysis of the MAGIC data, theoretical modelling, leadership of the publication effort, drafting and edition of the manuscript; P. Valisa: collection and analysis of the optical photometry data. The rest of the authors have contributed in one or several of the following ways: design, construction, maintenance and operation of the instrument(s) used to acquire the data; preparation and/or evaluation of the observation proposals; data acquisition, processing, calibration and/or reduction; production of analysis tools and/or related Monte Carlo simulations; discussion and approval of the contents of the draft.

Competing Interests: The authors declare that they have no competing interests.

Figure Legends/Captions

Fig. 1 Multiwavelength light curve of RS Oph. The figure shows the VHE (MAGIC, top panel), high-energy (*Fermi*-LAT, middle panel) and optical (TJO, ANS, and AAVSO, bottom panel) bands. The lack of MAGIC data between MJD 59440 and MJD 59454 is due to the presence of bad weather conditions and strong moonlight. Error bars represent 1-sigma statistical uncertainties in the data points.

Fig. 2 Schematic representation of RS Oph during an outburst. A photosphere (yellow circle) surrounds the white dwarf (WD, white small circle). Its companion star, a red giant (RG, red circle) emits a slow wind (red arrows). Ejecta of the nova explosion (grey arrows) propagate into the surrounding medium causing a shock wave encompassing the binary system (grey dashed line). In the shock wave, energetic electrons and protons (magenta and green wavy lines, respectively) are trapped by a magnetic field and accelerated. Gamma rays (white arrows) are produced by either electrons scattering the thermal radiation of the photosphere (yellow arrow) or by protons interacting with the surrounding matter (gray and red dots).

Fig. 3 Gamma-ray spectrum of RS Oph observed over the first four days of the outburst, and modeled with both a hadronic and leptonic scenario. *Fermi*-LAT observations are given by empty crosses and MAGIC by filled circles, averaged over the first four days of the outburst. The left panel shows a hadronic model; the right panel leptonic. The dashed line shows the gamma rays from the π^0 decay and the dotted line shows the inverse Compton contribution of the secondary $e^{\pm}$ pairs produced in hadronic interactions. dN/dE_p and dN/dE_e report the shape of the proton and electron energy distributions obtained from the fit. The bottom panel shows the fit residuals. Errorbars represent 1-sigma statistical uncertainties in the data points.

Fig. 4 Total energy versus duration of RS Oph 2021 outburst compared to that of the other novae detected by *Fermi*-LAT. Data taken from [14, 15, 68]. Errorbars represent 1-sigma statistical uncertainties in the data points.

References

[1] Bode, M.F., Evans, A.: Classical Novae vol. 43, (2008)

[2] Chomiuk, L., Metzger, B.D., Shen, K.J.: New insights into classical novae. Annual Review of Astronomy and Astrophysics **59**(1), 391–444 (2021)

[3] Townsley, D.M., Bildsten, L.: Theoretical Modeling of the Thermal State of Accreting White Dwarfs Undergoing Classical Nova Cycles. Astrophys. J. **600**(1), 390–403 (2004)

[4] Mikołajewska, J.: Symbiotic Stars: Observations Confront Theory. Baltic Astronomy **21**, 5–12 (2012)

[5] Ford, H.C.: The number of outbursts of a classical nova. Astrophys. J. **219**, 595 (1978).

[6] Schaefer, B.E.: Comprehensive Photometric Histories of All Known Galactic Recurrent Novae. Astrophys. J. Suppl. Ser. **187**(2), 275–373 (2010)

[7] Webbink, R.F., Livio, M., Truran, J.W., Orio, M.: The Nature of the Recurrent Novae. Astrophys. J. **314**, 653 (1987).

[8] Mikolajewska, J.: The Place of Recurrent Novae Among the Symbiotic Stars. In: Evans, A., Bode, M.F., O'Brien, T.J., Darnley, M.J. (eds.) RS Ophiuchi (2006) and the Recurrent Nova Phenomenon. Astronomical Society of the Pacific Conference Series, vol. 401, p. 42 (2008)

[9] Chen, W., Shrader, C.R., Livio, M.: The Properties of X-Ray and Optical Light Curves of X-Ray Novae. Astrophys. J. **491**(1), 312–338 (1997)

[10] Sokoloski, J.L., Luna, G.J.M., Mukai, K., Kenyon, S.J.: An X-ray-emitting blast wave from the recurrent nova RS Ophiuchi. Nature **442**(7100), 276–278 (2006)

[11] Bode, M.F., O'Brien, T.J., Osborne, J.P., Page, K.L., Senziani, F., Skinner, G.K., Starrfield, S., Ness, J.-U., Drake, J.J., Schwarz, G., Beardmore, A.P., Darnley, M.J., Eyres, S.P.S., Evans, A., Gehrels, N., Goad, M.R., Jean, P., Krautter, J., Novara, G.: Swift Observations of the 2006 Outburst of the Recurrent Nova RS Ophiuchi. I. Early X-Ray Emission from the Shocked Ejecta and Red Giant Wind. Astrophys. J. **652**(1), 629–635 (2006)

[12] Ness, J.-U., Starrfield, S., Beardmore, A.P., Bode, M.F., Drake, J.J., Evans, A., Gehrz, R.D., Goad, M.R., Gonzalez-Riestra, R., Hauschildt, P., Krautter, J., O'Brien, T.J., Osborne, J.P., Page, K.L., Schönrich, R.A.,

Woodward, C.E.: The SSS Phase of RS Ophiuchi Observed with Chandra and XMM-Newton. I. Data and Preliminary Modeling. Astrophys. J. **665**(2), 1334–1348 (2007)

[13] Nelson, T., Orio, M., Cassinelli, J.P., Still, M., Leibowitz, E., Mucciarelli, P.: X-Ray Spectroscopy of the 2006 Outburst of RS Ophiuchi. Astrophys. J. **673**(2), 1067–1079 (2008)

[14] Abdo, A.A., et al.: Gamma-Ray Emission Concurrent with the Nova in the Symbiotic Binary V407 Cygni. Science **329**(5993), 817–821 (2010)

[15] Ackermann, M., et al.: Fermi establishes classical novae as a distinct class of gamma-ray sources. Science **345**(6196), 554–558 (2014)

[16] Aliu, E., et al.: VERITAS Observations of the Nova in V407 Cygni. Astrophys. J. **754**(1), 77 (2012)

[17] Ahnen, M.L., et al.: Very high-energy γ-ray observations of novae and dwarf novae with the MAGIC telescopes. Astron. Astrophys. **582**, 67 (2015)

[18] Geary, K.: Outburst of RS Ophiuchi. vsnet-alert **26131** (2021)

[19] Cheung, C.C., Ciprini, S., Johnson, T.J.: Fermi-LAT Gamma-ray Detection of the Recurrent Nova RS Oph. The Astronomer's Telegram **14834**, 1 (2021)

[20] Wagner, S.J., H. E. S. S. Collaboration: Detection of VHE gamma-ray emission from the recurrent nova RS Ophiuchi with H.E.S.S. The Astronomer's Telegram **14844**, 1 (2021)

[21] Martin, P., Dubus, G., Jean, P., Tatischeff, V., Dosne, C.: Gamma-ray emission from internal shocks in novae. Astron. Astrophys. **612**, 38 (2018)

[22] Aydi, E., et al.: Direct evidence for shock-powered optical emission in a nova. Nature Astronomy **4**, 776–780 (2020)

[23] Sitarek, J., Bednarek, W.: GeV-TeV gamma rays and neutrinos from the Nova V407 Cygni. Phys. Rev. D **86**(6), 063011 (2012)

[24] Akaike, H.: A New Look at the Statistical Model Identification. IEEE Transactions on Automatic Control **19**, 716–723 (1974)

[25] Metzger, B.D., Caprioli, D., Vurm, I., Beloborodov, A.M., Bartos, I., Vlasov, A.: Novae as Tevatrons: prospects for CTA and IceCube. Mon. Not. R. Astron. Soc. **457**(2), 1786–1795 (2016)

[26] Shafter, A.W.: The Galactic Nova Rate Revisited. Astrophys. J. **834**(2),

196 (2017)

[27] Bath, G.T., Shaviv, G.: The space density, recurrence rate and classification of novae. Mon. Not. R. Astron. Soc. **183**, 515–522 (1978).

[28] Aleksić, J., et al.: The major upgrade of the MAGIC telescopes, Part I: The hardware improvements and the commissioning of the system. Astroparticle Physics **72**, 61–75 (2016)

[29] Aleksić, J., et al.: The major upgrade of the MAGIC telescopes, Part II: A performance study using observations of the Crab Nebula. Astroparticle Physics **72**, 76–94 (2016)

[30] Zanin, R., Carmona, E., J., S., P., C., K., F., M., G., S., L., M., L., A., M., for the MAGIC collaboration: MARS, the MAGIC analysis and reconstruction software . In: Proc. of the 33th International Cosmic Ray Conference (ICRC), p. 773 (2013).

[31] MAGIC Collaboration, et al.: VHE gamma-ray detection of FSRQ QSO B1420+326 and modeling of its enhanced broadband state in 2020. Astron. Astrophys. **647**, 163 (2021)

[32] MAGIC Collaboration, Acciari, V.A., Ansoldi, S., Antonelli, L.A., Arbet Engels, A., Baack, D., Babić, A., Banerjee, B., Barres de Almeida, U., Barrio, J.A., Becerra González, J., Bednarek, W., Bellizzi, L., Bernardini, E., Berti, A., Besenrieder, J., Bhattacharyya, W., Bigongiari, C., Biland, A., Blanch, O., Bonnoli, G., Bošnjak, Ž., Busetto, G., Carosi, A., Carosi, R., Ceribella, G., Chai, Y., Chilingaryan, A., Cikota, S., Colak, S.M., Colin, U., Colombo, E., Contreras, J.L., Cortina, J., Covino, S., D'Amico, G., D'Elia, V., da Vela, P., Dazzi, F., de Angelis, A., de Lotto, B., Delfino, M., Delgado, J., Depaoli, D., di Pierro, F., di Venere, L., Do Souto Espiñeira, E., Dominis Prester, D., Donini, A., Dorner, D., Doro, M., Elsaesser, D., Fallah Ramazani, V., Fattorini, A., Fernández-Barral, A., Ferrara, G., Fidalgo, D., Foffano, L., Fonseca, M.V., Font, L., Fruck, C., Fukami, S., Gallozzi, S., García López, R.J., Garczarczyk, M., Gasparyan, S., Gaug, M., Giglietto, N., Giordano, F., Godinović, N., Green, D., Guberman, D., Hadasch, D., Hahn, A., Herrera, J., Hoang, J., Hrupec, D., Hütten, M., Inada, T., Inoue, S., Ishio, K., Iwamura, Y., Jouvin, L., Kerszberg, D., Kubo, H., Kushida, J., Lamastra, A., Lelas, D., Leone, F., Lindfors, E., Lombardi, S., Longo, F., López, M., López-Coto, R., López-Oramas, A., Loporchio, S., Machado de Oliveira Fraga, B., Maggio, C., Majumdar, P., Makariev, M., Mallamaci, M., Maneva, G., Manganaro, M., Mannheim, K., Maraschi, L., Mariotti, M., Martínez, M., Masuda, S., Mazin, D., Mićanović, S., Miceli, D., Minev, M., Miranda, J.M., Mirzoyan, R., Molina, E., Moralejo, A., Morcuende, D., Moreno, V., Moretti, E.,

Munar-Adrover, P., Neustroev, V., Nigro, C., Nilsson, K., Ninci, D., Nishijima, K., Noda, K., Nogués, L., Nöthe, M., Nozaki, S., Paiano, S., Palacio, J., Palatiello, M., Paneque, D., Paoletti, R., Paredes, J.M., Peñil, P., Peresano, M., Persic, M., Prada Moroni, P.G., Prandini, E., Puljak, I., Rhode, W., Ribó, M., Rico, J., Righi, C., Rugliancich, A., Saha, L., Sahakyan, N., Saito, T., Sakurai, S., Satalecka, K., Schmidt, K., Schweizer, T., Sitarek, J., Šnidarić, I., Sobczynska, D., Somero, A., Stamerra, A., Strom, D., Strzys, M., Suda, Y., Surić, T., Takahashi, M., Tavecchio, F., Temnikov, P., Terzić, T., Teshima, M., Torres-Albà, N., Tosti, L., Tsujimoto, S., Vagelli, V., van Scherpenberg, J., Vanzo, G., Vazquez Acosta, M., Vigorito, C.F., Vitale, V., Vovk, I., Will, M., Zarić, D., Nava, L.: Teraelectronvolt emission from the γ-ray burst GRB 190114C. Nature **575**(7783), 455–458 (2019)

[33] Atwood, W.B., et al.: The Large Area Telescope on the Fermi Gamma-Ray Space Telescope Mission. Astrophys. J. **697**(2), 1071–1102 (2009)

[34] Wood, M., Caputo, R., Charles, E., Di Mauro, M., Magill, J., Perkins, J.S., Fermi-LAT Collaboration: Fermipy: An open-source Python package for analysis of Fermi-LAT Data. In: 35th International Cosmic Ray Conference (ICRC2017). International Cosmic Ray Conference, vol. 301, p. 824 (2017)

[35] Abdollahi, S., et al.: Fermi large area telescope fourth source catalog. The Astrophysical Journal Supplement Series **247**(1), 33 (2020).

[36] Ballet, J., Burnett, T.H., Digel, S.W., Lott, B.: Fermi Large Area Telescope Fourth Source Catalog Data Release 2. arXiv e-prints, 2005–11208 (2020)

[37] Mattox, J.R., et al.: The Likelihood Analysis of EGRET Data. Astrophys. J. **461**, 396 (1996).

[38] Principe, G., Malyshev, D., Ballet, J., Funk, S.: The first catalog of Fermi-LAT sources below 100 MeV. Astron. Astrophys. **618**, 22 (2018)

[39] Nilsson, K., et al.: Long-term optical monitoring of TeV emitting blazars. I. Data analysis. Astron. Astrophys. **620**, 185 (2018)

[40] Munari, U., et al.: The ANS Collaboration Monitoring Program. Baltic Astronomy **21**, 13–21 (2012).

[41] Munari, U., Moretti, S.: Characterizing the Photometric Response of the ANS Collaboration Monitoring Program. Baltic Astronomy **21**, 22–31 (2012).

[42] Henden, A.A., Levine, S.E., Terrell, D., Smith, T.C., Welch, D.: Data

Release 3 of the AAVSO All-Sky Photometric Survey (APASS). JAAVSO **40**(1), 430 (2012)

[43] Henden, A., Munari, U.: The APASS all-sky, multi-epoch BVgri photometric survey. Contributions of the Astronomical Observatory Skalnate Pleso **43**(3), 518–522 (2014)

[44] Landolt, A.U.: UBVRI Photometric Standard Stars Around the Celestial Equator: Updates and Additions. Astron. J. **137**(5), 4186–4269 (2009)

[45] Munari, U., Henden, A., Frigo, A., Dallaporta, S.: APASS discovery and characterization of 180 variable stars in Aquarius. Journal of Astronomical Data **20**, 4 (2014)

[46] Munari, U., et al.: APASS Landolt-Sloan BVgri Photometry of RAVE Stars. I. Data, Effective Temperatures, and Reddenings. Astron. J. **148**(5), 81 (2014)

[47] Teyssier, F.: Eruptive stars monitoring and the ARAS database. Contributions of the Astronomical Observatory Skalnate Pleso **49**(2), 217–227 (2019)

[48] Hachisu, I., Kato, M.: The UBV Color Evolution of Classical Novae. I. Nova-giant Sequence in the Color-Color Diagram. Astrophys. J. **785**(2), 97 (2014)

[49] Cardelli, J.A., Clayton, G.C., Mathis, J.S.: The Relationship between Infrared, Optical, and Ultraviolet Extinction. Astrophys. J. **345**, 245 (1989).

[50] Bessell, M.S., Castelli, F., Plez, B.: Model atmospheres broad-band colors, bolometric corrections and temperature calibrations for O - M stars. Astron. Astrophys. **333**, 231–250 (1998)

[51] Chesneau, O., Nardetto, N., Millour, F., Hummel, C., Domiciano de Souza, A., Bonneau, D., Vannier, M., Rantakyrö, F., Spang, A., Malbet, F., Mourard, D., Bode, M.F., O'Brien, T.J., Skinner, G., Petrov, R.G., Stee, P., Tatulli, E., Vakili, F.: AMBER/VLTI interferometric observations of the recurrent Nova RS Ophiuchii 5.5 days after outburst. Astron. Astrophys. **464**(1), 119–126 (2007)

[52] Skopal, A.: Multiwavelength modeling the SED of supersoft X-ray sources. II. RS Ophiuchi: From the explosion to the SSS phase. New Astron. **36**, 128–138 (2015)

[53] Munari, U., Valisa, P.: The 2021 outburst of RS Oph. A pictorial atlas of the spectroscopic evolution: the first 18 days. arXiv e-prints, 2109–01101

(2021)

[54] Leone, F., et al.: A Method to Calibrate the High-resolution Catania Astrophysical Observatory Spectropolarimeter. Astron. J. **151**(5), 116 (2016).

[55] Catanzaro, G., et al.: CAOS spectroscopy of Am stars Kepler targets. Mon. Not. R. Astron. Soc. **451**(1), 184–195 (2015)

[56] Skopal, A., Pribulla, T., Buil, C., Vittone, A., Errico, L.: Non-spherical Mass Outflow from RS Ophiuchi During its 2006 Outburst. In: Evans, A., Bode, M.F., O'Brien, T.J., Darnley, M.J. (eds.) RS Ophiuchi (2006) and the Recurrent Nova Phenomenon. Astronomical Society of the Pacific Conference Series, vol. 401, p. 227 (2008)

[57] Mondal, A., Anupama, G.C., Kamath, U.S., Das, R., Selvakumar, G., Mondal, S.: Optical spectroscopy of the recurrent nova RS Ophiuchi - from the outburst of 2006 to quiescence. Mon. Not. R. Astron. Soc. **474**(3), 4211–4224 (2018)

[58] Ribeiro, V.A.R.M., et al.: The Expanding Nebular Remnant of the Recurrent Nova RS Ophiuchi (2006). II. Modeling of Combined Hubble Space Telescope Imaging and Ground-based Spectroscopy. Astrophys. J. **703**(2), 1955–1963 (2009)

[59] Sokoloski, J.L., Rupen, M.P., Mioduszewski, A.J.: Uncovering the Nature of Nova Jets: A Radio Image of Highly Collimated Outflows from RS Ophiuchi. Astrophys. J. Lett. **685**(2), 137 (2008).

[60] Bode, M.F., Harman, D.J., O'Brien, T.J., Bond, H.E., Starrfield, S., Darnley, M.J., Evans, A., Eyres, S.P.S.: Hubble Space Telescope Imaging of the Expanding Nebular Remnant of the 2006 Outburst of the Recurrent Nova RS Ophiuchi. Astrophys. J. Lett. **665**(1), 63–66 (2007)

[61] Booth, R.A., Mohamed, S., Podsiadlowski, P.: Modelling the circumstellar medium in RS Ophiuchi and its link to Type Ia supernovae. Mon. Not. R. Astron. Soc. **457**(1), 822–835 (2016)

[62] Moderski, R., Sikora, M., Coppi, P.S., Aharonian, F.: Klein-Nishina effects in the spectra of non-thermal sources immersed in external radiation fields. Mon. Not. R. Astron. Soc. **363**(3), 954–966 (2005)

[63] Walch, S., Naab, T.: The energy and momentum input of supernova explosions in structured and ionized molecular clouds. Mon. Not. R. Astron. Soc. **451**(3), 2757–2771 (2015)

[64] Rozwadowska, K., Vissani, F., Cappellaro, E.: On the rate of core collapse

supernovae in the milky way. New Astron. **83**, 101498 (2021)

[65] Webber, W.R.: A new estimate of the local interstellar energy density and ionization rate of galactic cosmic cosmic rays. The Astrophysical Journal **506**(1), 329–334 (1998).

[66] Buck, T., Pfrommer, C., Pakmor, R., Grand, R.J.J., Springel, V.: The effects of cosmic rays on the formation of Milky Way-mass galaxies in a cosmological context. Mon. Not. R. Astron. Soc. **497**(2), 1712–1737 (2020)

[67] Schaefer, B.E.: Orbital Periods for Three Recurrent Novae. Astrophys. J. **697**(1), 721–729 (2009)

[68] Cheung, C.C., et al.: Fermi-LAT Gamma-Ray Detections of Classical Novae V1369 Centauri 2013 and V5668 Sagittarii 2015. Astrophys. J. **826**(2), 142 (2016)

[69] Munari, U., et al.: The 2006 Outburst of the Recurrent Nova RS OPH. Baltic Astronomy **16**, 46–48 (2007)

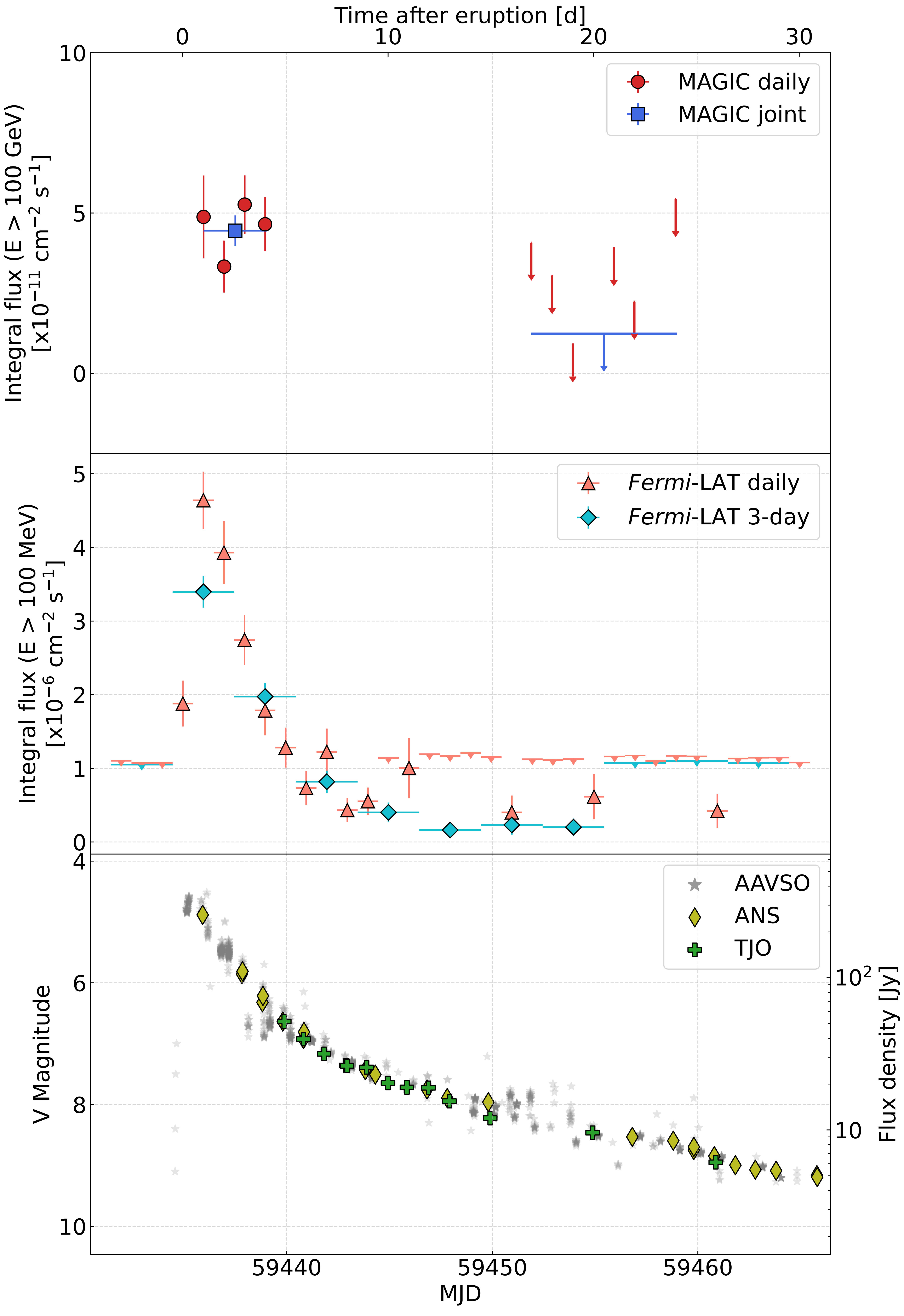
Time after eruption [d]
0
10
20
30
Integral flux (E > 100 GeV) [x10^{-11} cm^{-2} s^{-1}]
10
5
0
MAGIC daily
MAGIC joint
Integral flux (E > 100 MeV) [x10^{-6} cm^{-2} s^{-1}]
5
4
3
2
1
0
Fermi-LAT daily
Fermi-LAT 3-day
V Magnitude
4
6
8
10
Flux density [Jy]
10^2
10
AAVSO
ANS
TJO
59440
59450
59460
MJD

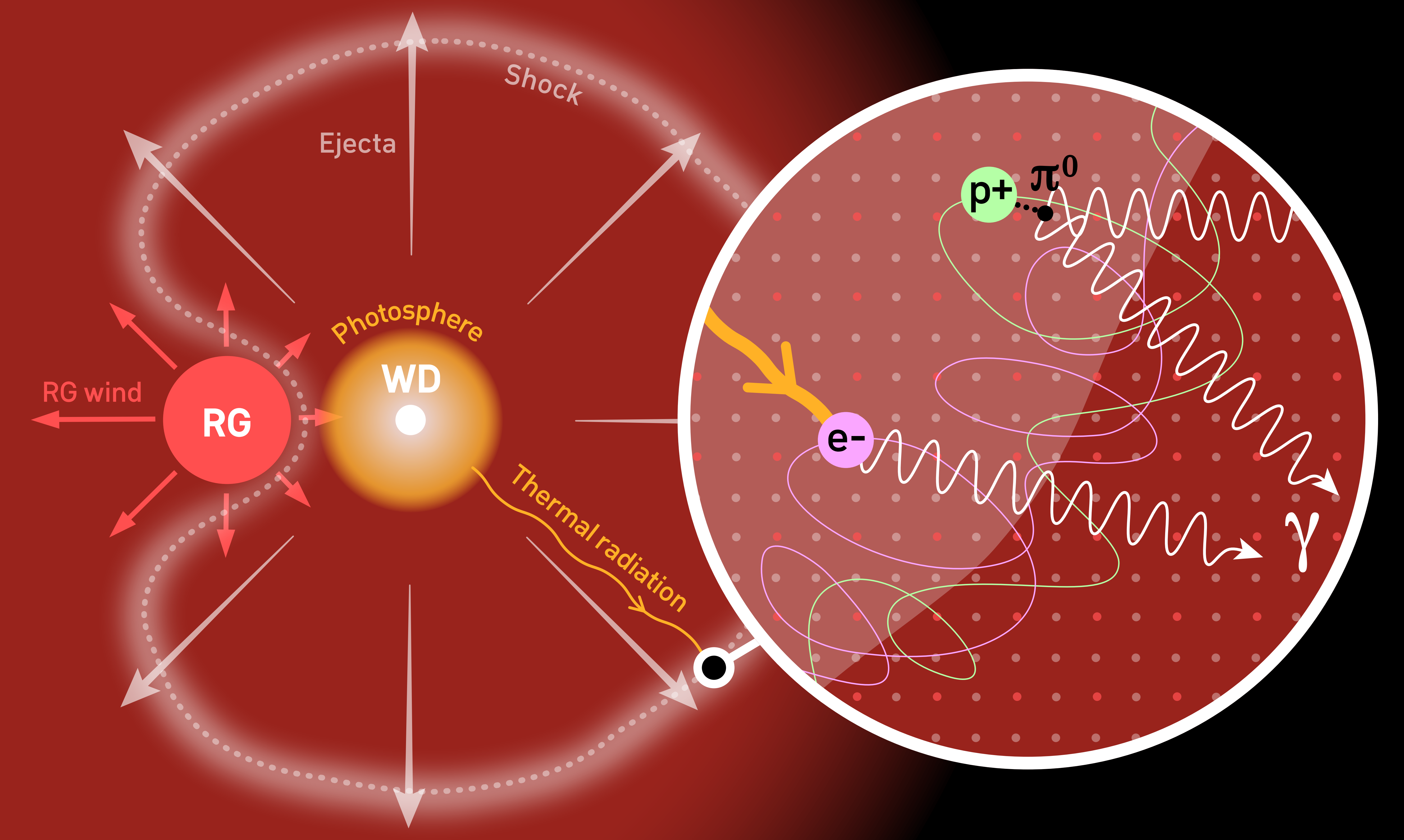
Shock
Ejecta
Photosphere
WD
RG wind
RG
Thermal radiation
p+
π^0
e-
γ

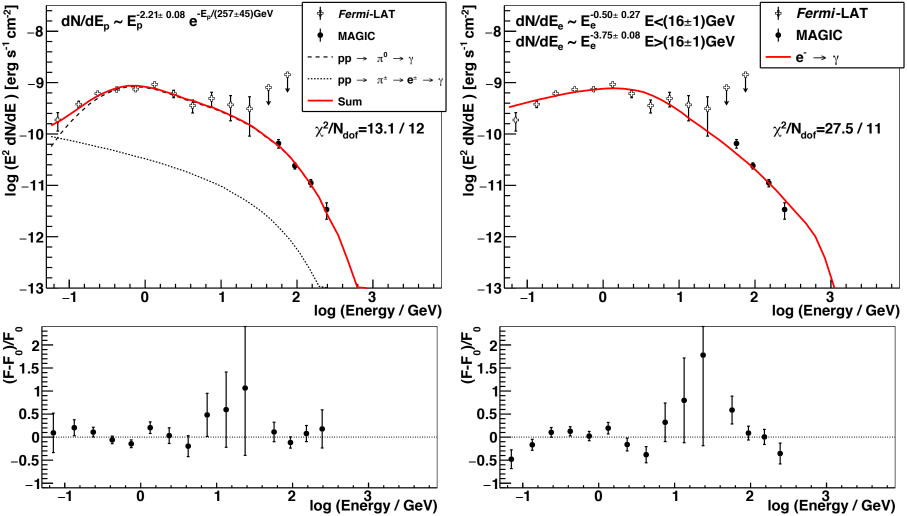
$dN/dE_p \sim E_p^{-2.21\pm 0.08}\, e^{-E_p/(257\pm45)\mathrm{GeV}}$
Fermi-LAT
MAGIC
pp → π^0 → γ
pp → $\pi^\pm$ → $e^\pm$ → γ
Sum
χ^2/N_{dof}=13.1 / 12
$dN/dE_e \sim E_e^{-0.50\pm 0.27}$ E<(16±1)GeV
$dN/dE_e \sim E_e^{-3.75\pm 0.08}$ E>(16±1)GeV
Fermi-LAT
MAGIC
e^- → γ
χ^2/N_{dof}=27.5 / 11
log (E^2 dN/dE) [erg s^{-1} cm^{-2}]
−8
−9
−10
−11
−12
−13
−1
0
1
2
3
log (Energy / GeV)
$(F-F_0)/F_0$
2
1.5
1
0.5
0
−0.5
−1

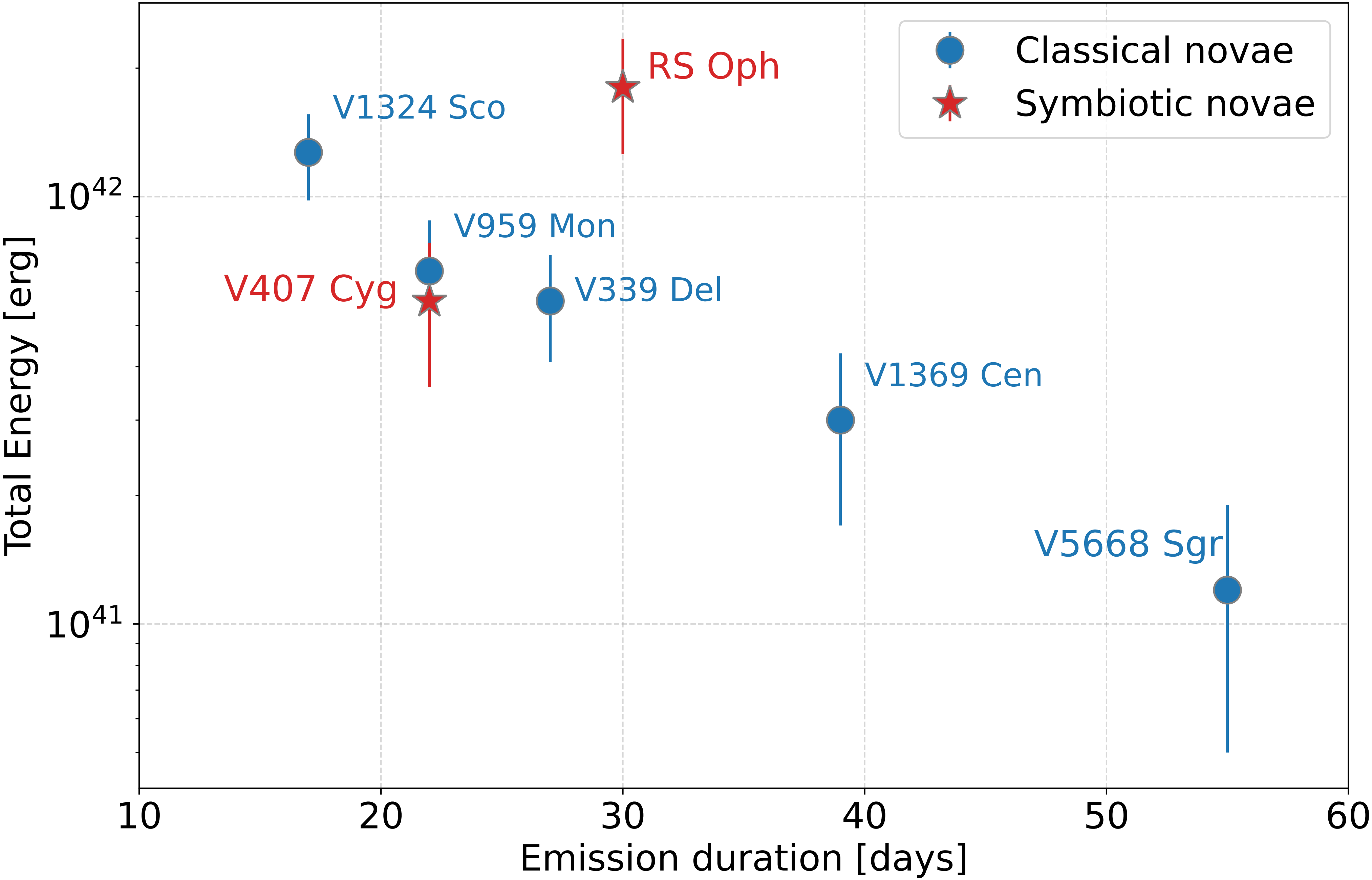
Classical novae
Symbiotic novae
RS Oph
V1324 Sco
V959 Mon
V407 Cyg
V339 Del
V1369 Cen
V5668 Sgr
Total Energy [erg]
10^{42}
10^{41}
10
20
30
40
50
60
Emission duration [days]

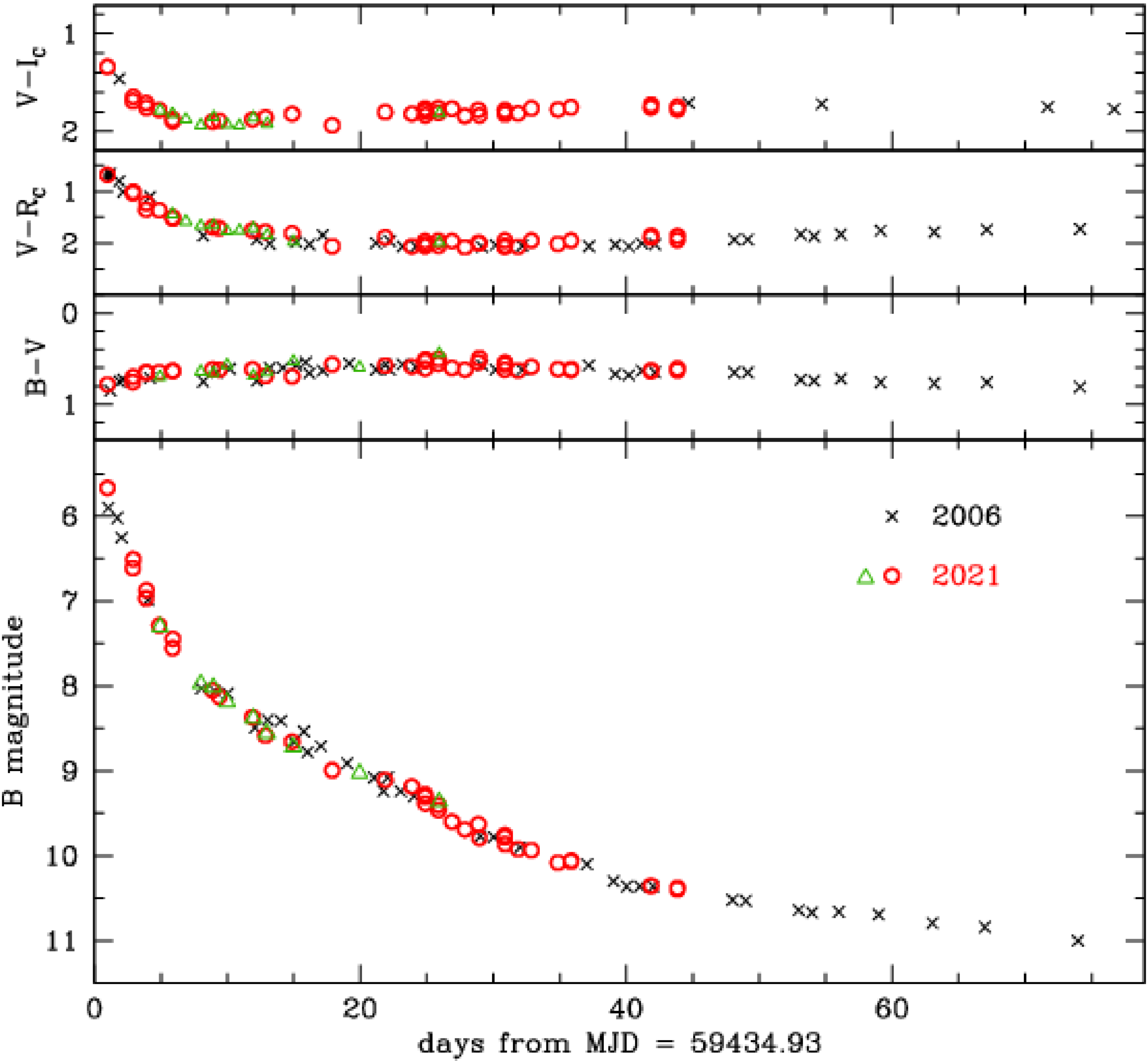
V−I$_c$
1
2
V−R$_c$
1
2
B−V
0
1
B magnitude
6
7
8
9
10
11
2006
2021
0
20
40
60
days from MJD = 59434.93

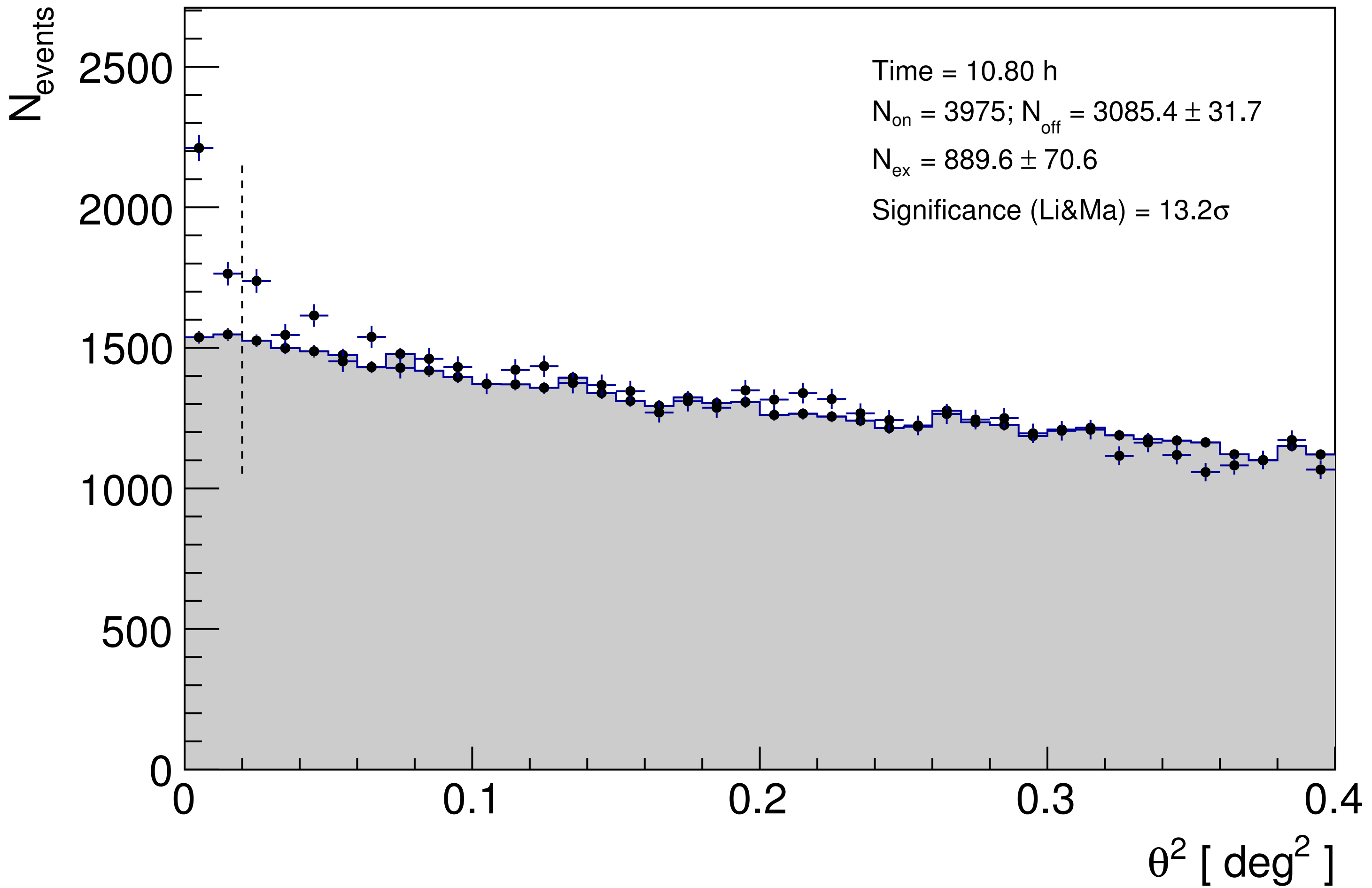
N_events
2500
2000
1500
1000
500
0
0
0.1
0.2
0.3
0.4
θ² [deg²]
Time = 10.80 h
N_on = 3975; N_off = 3085.4 ± 31.7
N_ex = 889.6 ± 70.6
Significance (Li&Ma) = 13.2σ

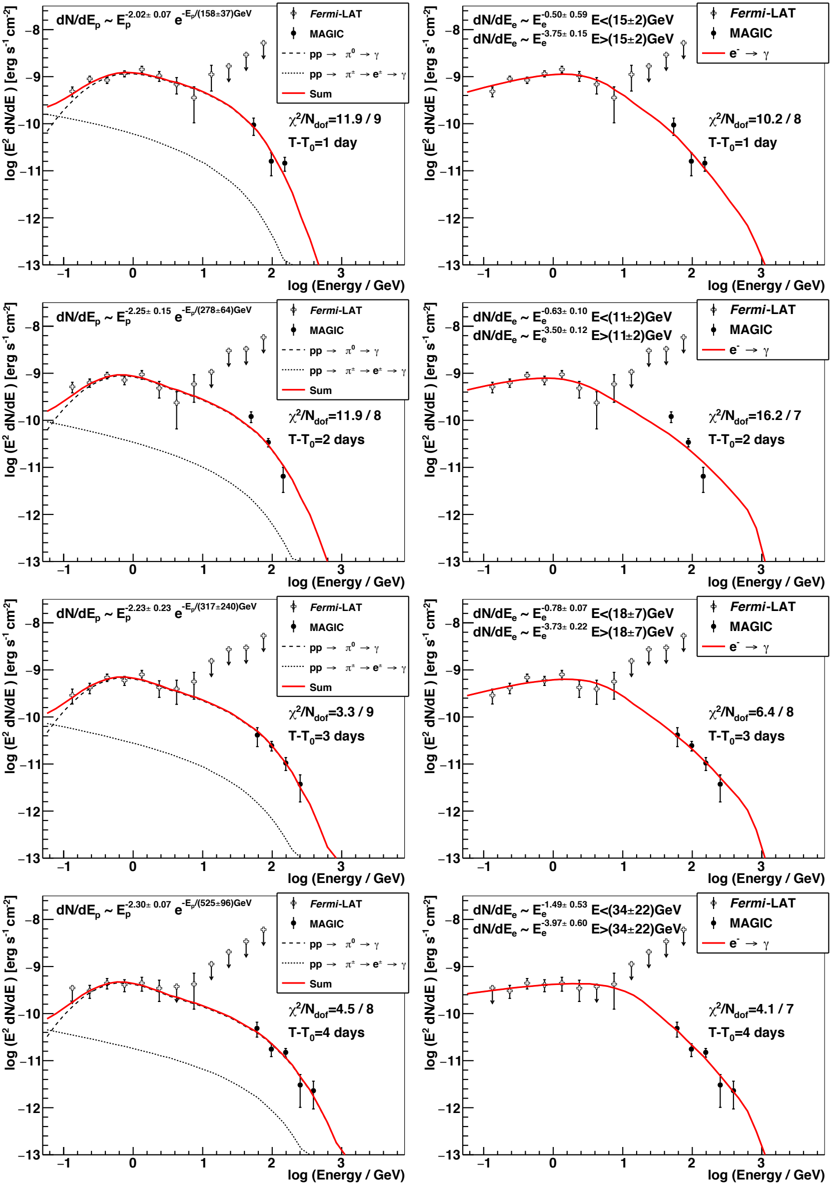
dN/dE$_p$ ~ E$_p^{-2.02\pm0.07}$ e$^{-E_p/(158\pm37)GeV}$
Fermi-LAT
MAGIC
pp → π⁰ → γ
pp → π± → e± → γ
Sum
χ²/N$_{dof}$=11.9 / 9
T-T$_0$=1 day
dN/dE$_e$ ~ E$_e^{-0.50\pm0.59}$ E<(15±2)GeV
dN/dE$_e$ ~ E$_e^{-3.75\pm0.15}$ E>(15±2)GeV
e⁻ → γ
χ²/N$_{dof}$=10.2 / 8
T-T$_0$=1 day
dN/dE$_p$ ~ E$_p^{-2.25\pm0.15}$ e$^{-E_p/(278\pm64)GeV}$
χ²/N$_{dof}$=11.9 / 8
T-T$_0$=2 days
dN/dE$_e$ ~ E$_e^{-0.63\pm0.10}$ E<(11±2)GeV
dN/dE$_e$ ~ E$_e^{-3.50\pm0.12}$ E>(11±2)GeV
χ²/N$_{dof}$=16.2 / 7
T-T$_0$=2 days
dN/dE$_p$ ~ E$_p^{-2.23\pm0.23}$ e$^{-E_p/(317\pm240)GeV}$
χ²/N$_{dof}$=3.3 / 9
T-T$_0$=3 days
dN/dE$_e$ ~ E$_e^{-0.78\pm0.07}$ E<(18±7)GeV
dN/dE$_e$ ~ E$_e^{-3.73\pm0.22}$ E>(18±7)GeV
χ²/N$_{dof}$=6.4 / 8
T-T$_0$=3 days
dN/dE$_p$ ~ E$_p^{-2.30\pm0.07}$ e$^{-E_p/(525\pm96)GeV}$
χ²/N$_{dof}$=4.5 / 8
T-T$_0$=4 days
dN/dE$_e$ ~ E$_e^{-1.49\pm0.53}$ E<(34±22)GeV
dN/dE$_e$ ~ E$_e^{-3.97\pm0.60}$ E>(34±22)GeV
χ²/N$_{dof}$=4.1 / 7
T-T$_0$=4 days
log (E² dN/dE) [erg s⁻¹ cm⁻²]
log (Energy / GeV)
−8
−9
−10
−11
−12
−13
−1
0
1
2
3

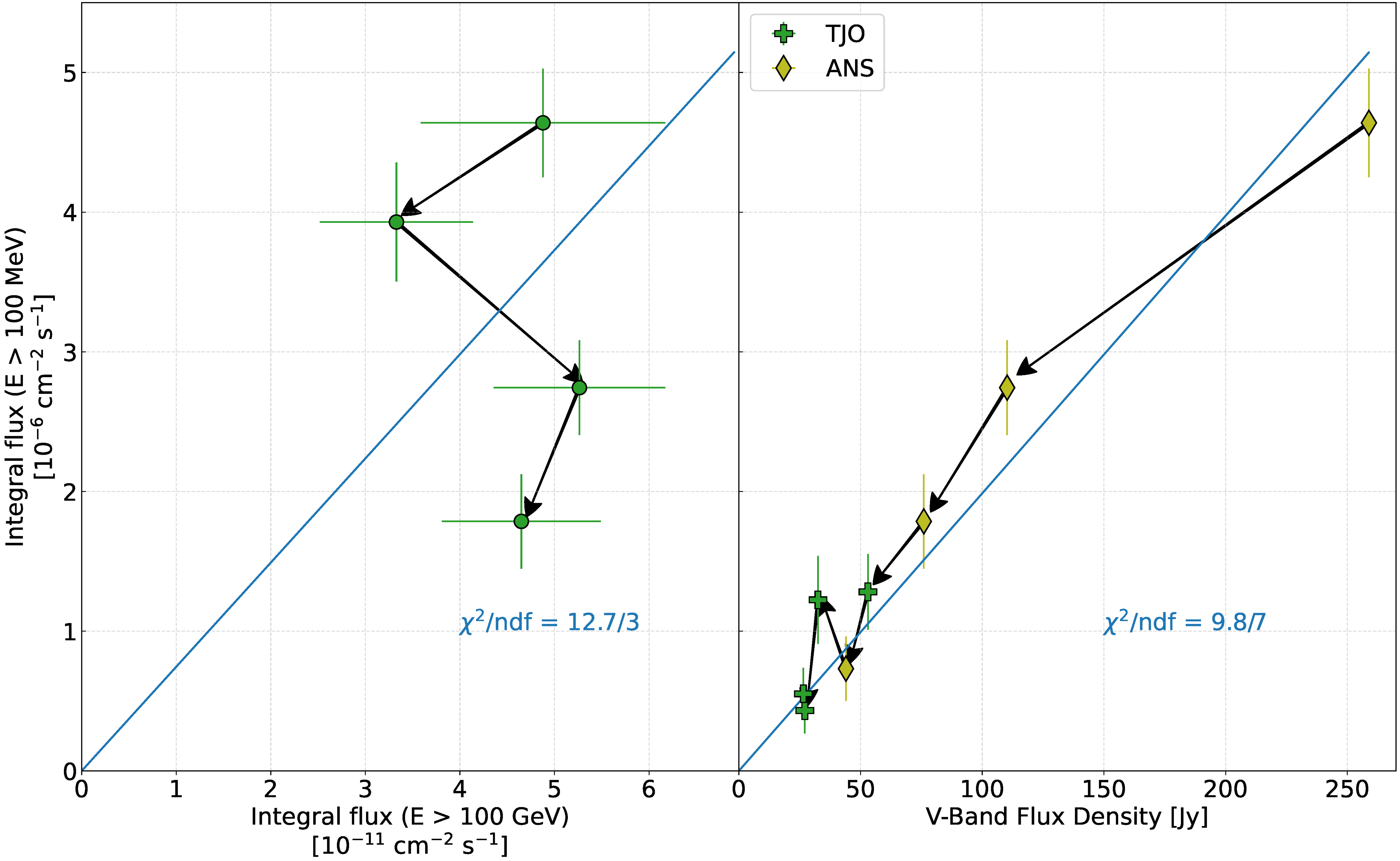
Integral flux (E > 100 MeV) [10⁻⁶ cm⁻² s⁻¹]
0
1
2
3
4
5
Integral flux (E > 100 GeV) [10⁻¹¹ cm⁻² s⁻¹]
0
1
2
3
4
5
6
χ²/ndf = 12.7/3
TJO
ANS
χ²/ndf = 9.8/7
V-Band Flux Density [Jy]
0
50
100
150
200
250

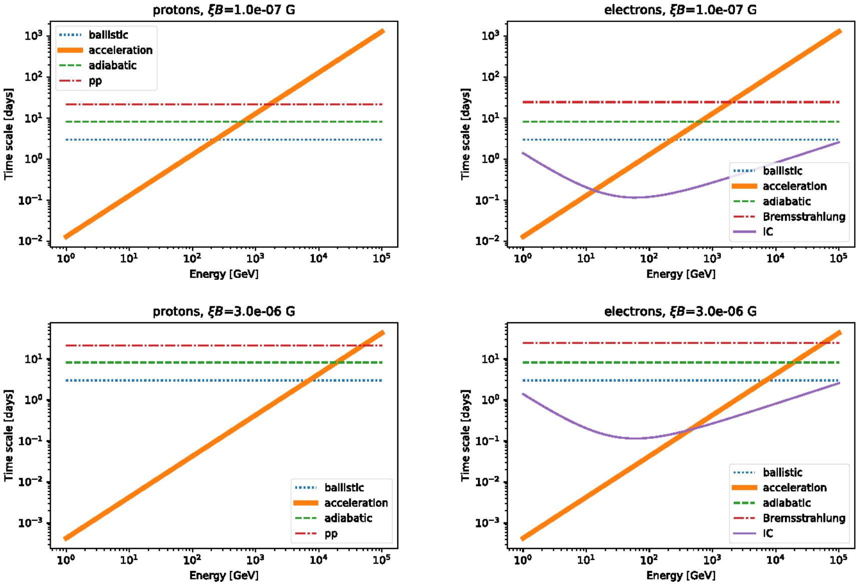
protons, ξB=1.0e-07 G
electrons, ξB=1.0e-07 G
protons, ξB=3.0e-06 G
electrons, ξB=3.0e-06 G
ballistic
acceleration
adiabatic
pp
Bremsstrahlung
IC
Time scale [days]
Energy [GeV]
10^{-3}
10^{-2}
10^{-1}
10^{0}
10^{1}
10^{2}
10^{3}
10^{4}
10^{5}

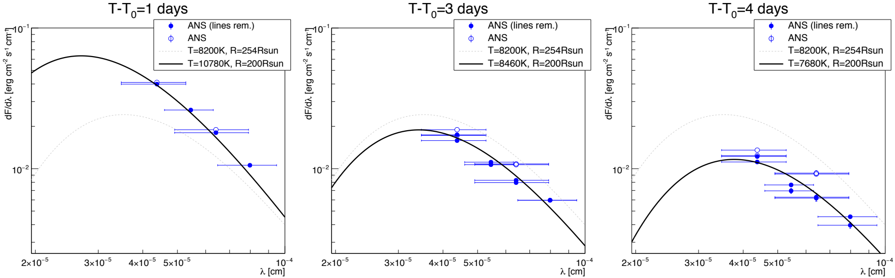
T-T$_0$=1 days
T-T$_0$=3 days
T-T$_0$=4 days
ANS (lines rem.)
ANS
T=8200K, R=254Rsun
T=10780K, R=200Rsun
T=8460K, R=200Rsun
T=7680K, R=200Rsun
dF/dλ [erg cm^{-2} s^{-1} cm^{-1}]
10^{-1}
10^{-2}
2×10^{-5}
3×10^{-5}
4×10^{-5}
5×10^{-5}
10^{-4}
λ [cm]

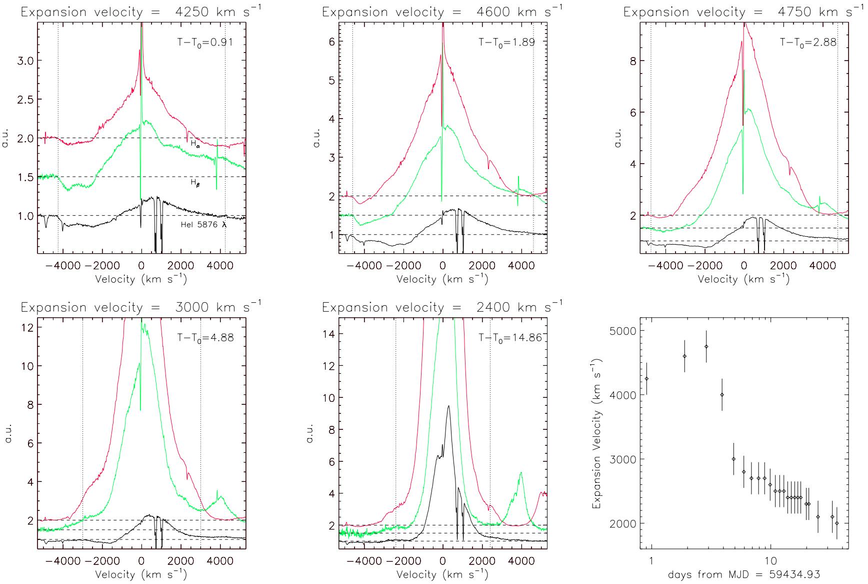
Expansion velocity = 4250 km s^{-1}
T−T$_0$=0.91
H$_\alpha$
H$_\beta$
HeI 5876 λ
Expansion velocity = 4600 km s^{-1}
T−T$_0$=1.89
Expansion velocity = 4750 km s^{-1}
T−T$_0$=2.88
Expansion velocity = 3000 km s^{-1}
T−T$_0$=4.88
Expansion velocity = 2400 km s^{-1}
T−T$_0$=14.86
a.u.
Velocity (km s^{-1})
−4000 −2000 0 2000 4000
Expansion Velocity (km s^{-1})
days from MJD = 59434.93
1
10
2000
3000
4000
5000

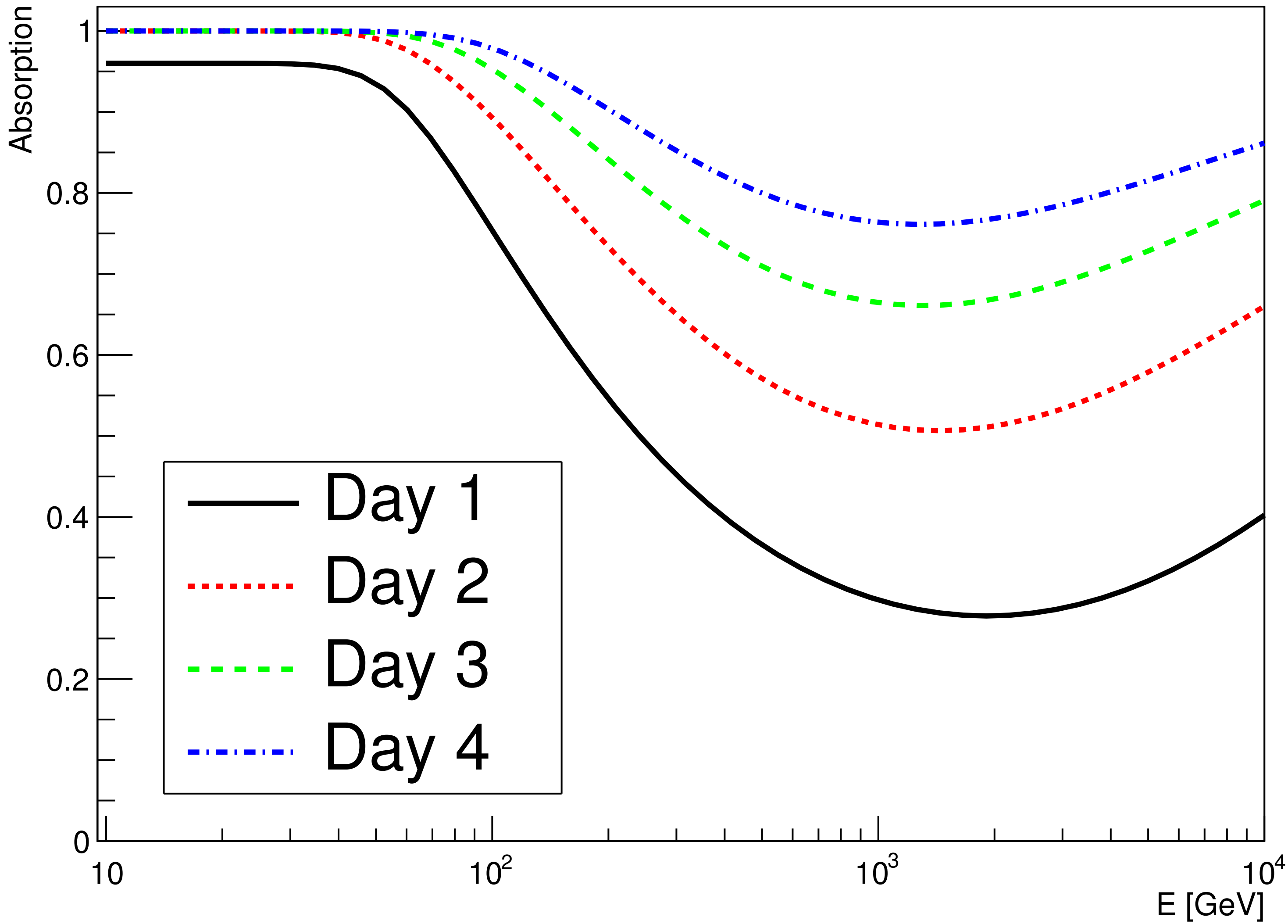
Absorption
1
0.8
0.6
0.4
0.2
0
10
10^2
10^3
10^4
E [GeV]
Day 1
Day 2
Day 3
Day 4

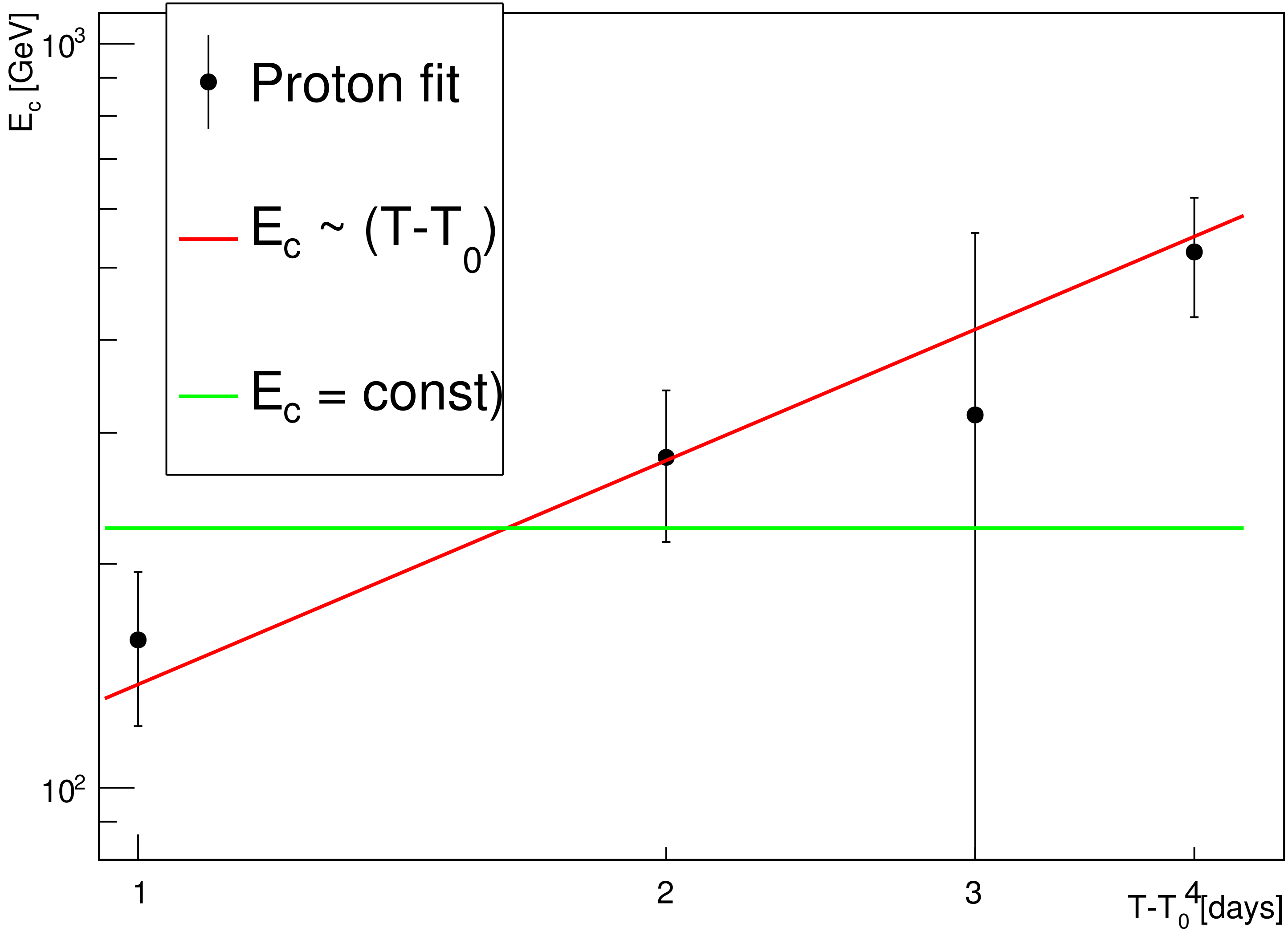
E_c [GeV]
10^3
10^2
1
2
3
4
T-T_0 [days]
Proton fit
E_c ~ (T-T_0)
E_c = const)

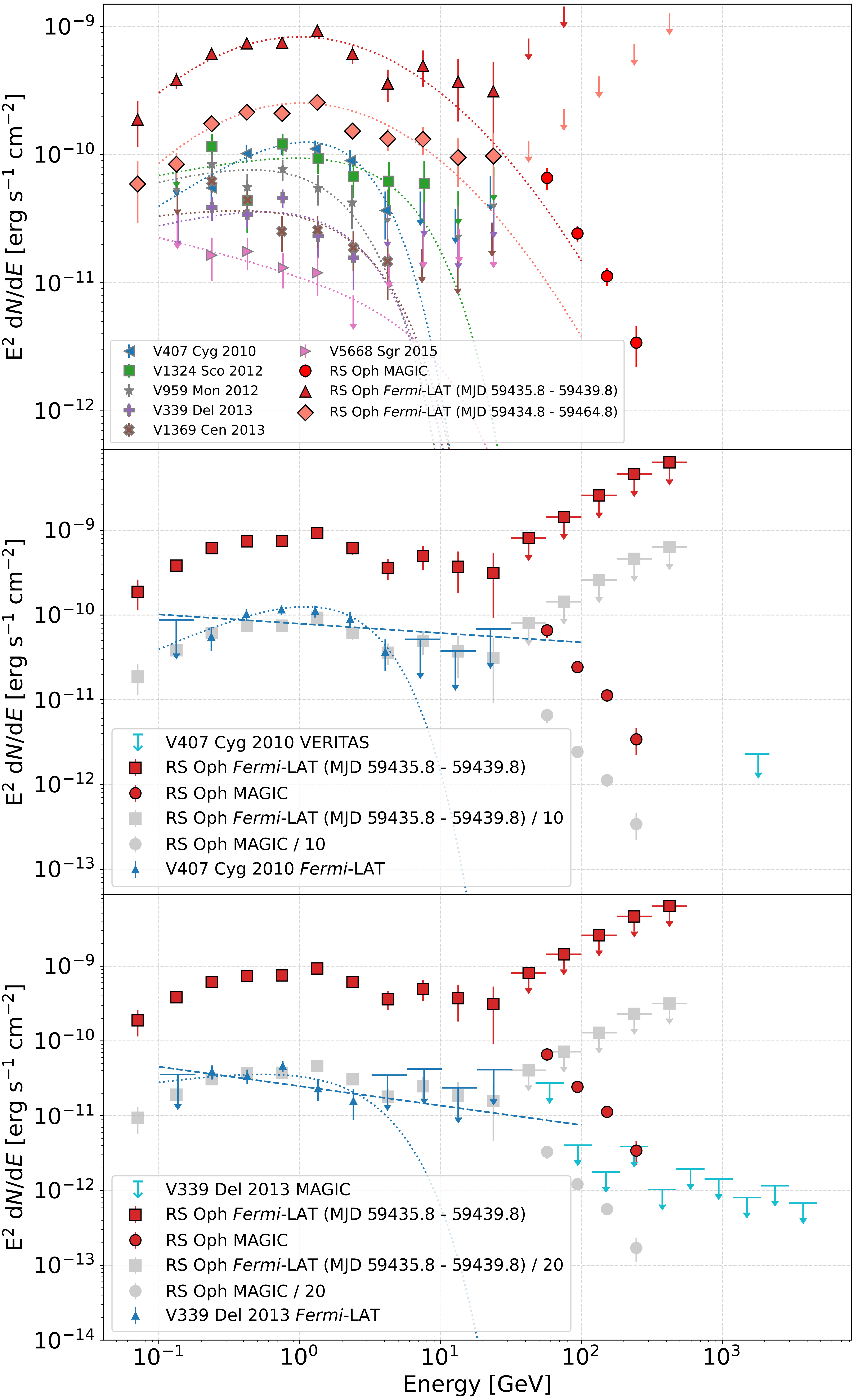
10^{-9}
10^{-10}
10^{-11}
10^{-12}
10^{-13}
10^{-14}
E^2 dN/dE [erg s^{-1} cm^{-2}]
V407 Cyg 2010
V1324 Sco 2012
V959 Mon 2012
V339 Del 2013
V1369 Cen 2013
V5668 Sgr 2015
RS Oph MAGIC
RS Oph *Fermi*-LAT (MJD 59435.8 - 59439.8)
RS Oph *Fermi*-LAT (MJD 59434.8 - 59464.8)
V407 Cyg 2010 VERITAS
RS Oph *Fermi*-LAT (MJD 59435.8 - 59439.8)
RS Oph MAGIC
RS Oph *Fermi*-LAT (MJD 59435.8 - 59439.8) / 10
RS Oph MAGIC / 10
V407 Cyg 2010 *Fermi*-LAT
V339 Del 2013 MAGIC
RS Oph *Fermi*-LAT (MJD 59435.8 - 59439.8)
RS Oph MAGIC
RS Oph *Fermi*-LAT (MJD 59435.8 - 59439.8) / 20
RS Oph MAGIC / 20
V339 Del 2013 *Fermi*-LAT
10^{-1}
10^{0}
10^{1}
10^{2}
10^{3}
Energy [GeV]